



Contents lists available at ScienceDirect

# Journal of the Mechanical Behavior of Biomedical Materials

journal homepage: [www.elsevier.com/locate/jmbbm](http://www.elsevier.com/locate/jmbbm)

## Effect of mechanical stimulation on the degradation of poly(lactic acid) scaffolds with different designed structures

Hengtao Shui<sup>a</sup>, Quan Shi<sup>a</sup>, Nicola M. Pugno<sup>b,c,d</sup>, Qiang Chen<sup>a,\*</sup>, Zhiyong Li<sup>a,e,\*\*</sup><sup>a</sup> Biomechanics Laboratory, School of Biological Science & Medical Engineering, Southeast University, 210096, Nanjing, PR China<sup>b</sup> Laboratory of Bio-Inspired & Graphene Nanomechanics, Department of Civil, Environmental and Mechanical Engineering, University of Trento, I-38123, Trento, Italy<sup>c</sup> School of Engineering and Materials Science, Queen Mary University of London, Mile End Road, E14NS, London, UK<sup>d</sup> Ket Lab, Edoardo Amaldi Foundation, Via del Politecnico snc, I-11, 00133, Rome, Italy<sup>e</sup> School of Chemistry, Physics and Mechanical Engineering, Queensland University of Technology (QUT), Brisbane, QLD, 4001, Australia

## ARTICLE INFO

## Keywords:

Scaffold degradation  
Mechanical stimulation  
Autocatalysis  
Mathematical modeling  
Finite element method

## ABSTRACT

Biodegradability is one of the required scaffold functions for bone tissue engineering, and it is influenced by the mechanical micro-environment after scaffold implantation into body. This paper aimed to develop a mathematical model to numerically study the mechanical impact on the degradation of poly (lactic acid) (PLA) scaffolds with different designed structures. In addition, the diffusion-governed autocatalysis on the scaffold degradation was also included, and the scaffold collapse time by an author-developed algorithm was determined. The results showed that an increase in mechanical stimulation led to an increase in the scaffold degradation rate. Moreover, different structures with a similar porosity shared a degradation tendency but had different collapse times, which was very sensitive to the diffusion coefficient of the scaffold. The present study could be helpful to understand the dynamic degradation process of PLA scaffolds, and guide the design of PLA material and scaffold structure. It may be also used as a tool for the evaluation of the *in vitro* and *in vivo* degradation performance of scaffolds.

## 1. Introduction

Scaffold as one of three key factors in bone tissue engineering (Kang et al., 2009) should have: (i) three-dimensional porous structure for cell growth and transport of nutrients; (ii) biocompatibility and biodegradability with a controllable degradation rate to match bone formation rate; (iii) sufficient stiffness and strength to sustain the external load during the whole bone-repair process (Rose and Oreffo, 2002; Hutmacher, 2000; Zhang and Ma, 1999; Mi et al., 2015, 2018). Polymer is one of several biomaterials, and often employed to construct scaffolds. Thus, it has drawn much attention for biomedical applications due to its excellent processability and biodegradability (Su et al., 2018; Helder et al., 1990).

The degradation of ester polymers is mainly caused by the hydrolysis, which is influenced by many factors, such as pH value (Zolnik and Burgess, 2007), temperature, crystallinity (Tsuji et al., 2015), autocatalysis (Siepmann et al., 2005), loads (Fan et al., 2008) and loading frequency (Kang et al., 2009; Nicodemus et al., 2009). The hydrolysis causes the chain scission in polymer matrix, and this embodies the

decreases of the molecular weight, mechanical properties, mass and volumetric shrinkage of the polymer (Göpferich, 1996). Extensive experimental studies have been conducted to explore the degradation mechanism of bulk polymer influenced by these factors. In particular, compared to the unloaded polymer, load was proved to accelerate the polymer degradation (Fan et al., 2008), moreover, the loading intensity and frequency influenced the bulk polymer degradation. For porous polymer scaffolds, a higher porosity induced a severer loss of mass, molecular weight and compressive modulus (Zhang et al., 2013), and pore morphologies also influenced the polymer degradation (Wu and Ding, 2010). In addition, the porous scaffolds are subjected to the mechanical stimulation after being implanted into human body, and according to the loading effect on the bulk polymer degradation, the mechanical stimulation must affect the degradation of the porous polymer scaffolds. Thus, both the architecture of porous scaffolds and the mechanical stimulation should be considered to design scaffolds except the well-studied chemical factors on the degradation of bulk polymers, and it is necessary to study the degradation of porous scaffolds with different architectures under mechanical stimulation.

\* Corresponding author.

\*\* Corresponding author. Biomechanics Laboratory, School of Biological Science & Medical Engineering, Southeast University, 210096, Nanjing, PR China.  
E-mail addresses: [chenq999@gmail.com](mailto:chenq999@gmail.com) (Q. Chen), [zylicam@gmail.com](mailto:zylicam@gmail.com) (Z. Li).

<https://doi.org/10.1016/j.jmbbm.2019.04.028>

Received 16 January 2019; Received in revised form 12 April 2019; Accepted 16 April 2019

Available online 18 April 2019

1751-6161/ © 2019 Elsevier Ltd. All rights reserved.

Computational modeling and numerical simulation are useful techniques to evaluate the bulk polymer degradation. In this sense, many theoretical or numerical frameworks have been developed on the degradation (Sackett and Narasimhan, 2011; Han and Pan, 2009; Zhang et al., 2017). In general, there are two main kinds of mathematical models to describe the degradation. The first is probabilistic model, which was developed on the basis of the random chain scission of polymer. The model includes Erlang probability density function (Göpferich, 1996; von Burkersroda et al., 2002; Göpferich and Langer, 1993), Monte Carlo (MC) (Bose and Git, 2004), and cellular automata (CA) methods (Arifin et al., 2006). In particular, the Erlang probability density function is popularly used to describe the bulk degradation of polymers. For example, Chen et al. (2011) combined stochastic hydrolysis and mass transport to simulate the polymer degradation, and the model result showed a good agreement with experimental findings. The second is phenomenological model, which is based on mechanistic phenomena, such as autocatalytic reaction and crystallinity. For the autocatalysis, it is induced by the high concentration of carboxyl end groups released in the hydrolytic course, and the hydrolytic product cannot be timely diffused out of the polymer matrix (Siparsky et al., 1998). Furthermore, as a catalyst, the acidic hydrolytic product effectively increased the local degradation rate of bulk polymers (Chen et al., 2011). Antheunis et al. (2010) developed a degradation model containing autocatalytic effect and predicted the average molecular weight of aliphatic polyesters during hydrolysis.

In order to address the architectural effect of porous scaffolds and the mechanical impact on the degradation of polymer scaffolds, this paper aims to develop a mathematical model (including the first-order Erlang stochastic hydrolysis, autocatalytic and loading effects) to explore the degradation kinetics of different scaffold architectures by employing the effective numerical method. Here, we designed three representative volumetric cells (RVCs) of three periodic scaffolds, which could be fabricated by the computer assisted design (CAD) and 3D-printing techniques (Gómez et al., 2016). By combining the developed mathematical model with the finite element method, the effect of the mechanical stimulation on the degradation of the RVCs was studied.

## 2. Degradation theory

### 2.1. Polymer stochastic hydrolysis

In hydrolysis, water molecules attack and break long polymer chains into water soluble products, resulting in the decrease of the molecular weight. Experiments have verified that the polymer degradation follows the pseudo-first-order kinetics (Göpferich, 1997), and a ratio  $\beta(t)$  is defined to describe normalized number average molecular weight (Shi et al., 2018):

$$\beta(t) = \frac{M_n(t)}{M_n(0)} = e^{-\lambda_0 t} \quad (1)$$

where  $M_n(0)$  and  $M_n(t)$  are the initial ( $t = 0$ ) and instantaneous number average molecular weight,  $\lambda_0$  is the degradation rate constant of polymer which is determined by the polymer components. Ideally, the polymer is considered to be isotropic, and all material points (here, a material point corresponds to a scaffold element in the following numerical models, hereafter, scaffold element is used) share an initial  $M_n(0)$ . However, scaffold elements have different initial porosities  $\alpha$  caused by the hydrolysis due to environment humidity, here it is randomly assigned a value between 0 and 0.2. The degradation process of the scaffold element can be considered with a delay  $t_{add}$ , which is calculated from Eq. (1) as (Bose and Git, 2004):

$$t_{add} = -\frac{\ln(1 - \alpha)}{\lambda_0} \quad (2)$$

According to Göpferich et al. (1997), the bulk degradation of polymer was a stochastic process, and each scaffold element was

considered as a stochastic event. The normalized number average molecular weight described in Eq. (1) corresponds to the first-order Erlang stochastic process, and the probability density function  $p(t)$  for each scaffold element is defined as:

$$p(t) = k\lambda_0 e^{-k\lambda_0 t} \quad (3)$$

with

$$k = \frac{\ln(n)}{\ln(m)}$$

where  $n$  is the element number of the RVC in the present work, and  $m$  is the referred element number of the RVC in (Bose and Git, 2004). It is worth mentioning that  $k$  is a coefficient considering the size effect, since the number of scaffold element influences the degradation. Namely, the smaller  $n$  (or the larger element size), the smaller the degradation probability of a scaffold element, and this requires a longer time for a complete degradation of scaffold elements (Göpferich, 1997).

### 2.2. Inclusion of mechanical stimulation into the stochastic hydrolysis

Experiments revealed the effect of the mechanical stimulation on the polymer degradation (Thompson et al., 1996; Li et al., 2017a). In order to incorporate the mechanical stimulation into the degradation model, the degradation rate was re-expressed on the basis of an analysis on atomic fracture mechanism of solid polymers, and the refined degradation rate  $\lambda_\sigma$  was proposed by Zhurkov et al. (1974) as:

$$\lambda_\sigma = A e^{-\frac{E_A - B\sigma}{RT}} \quad (4)$$

where  $A$  is the Arrhenius frequency factor,  $E_A$  is the activation energy breaking polymer chains,  $\sigma$  is the externally applied stress,  $B$  is a coefficient,  $R$  is molar gas constant and  $T$  is Kelvin temperature. Eq. (4) shows that the applied stress decreases the activation energy, and thus accelerates the polymer degradation. In particular, when  $\sigma$  is zero, Eq. (4) shrinks to the Arrhenius' equation, then  $\lambda_\sigma = \lambda_0$ . Assuming that the temperature during the hydrolysis is constant, Eq. (4) is re-written as:

$$\lambda_\sigma = A e^{-\frac{E_A - B\sigma}{RT}} = \lambda_0 e^{\frac{B\sigma}{RT}} \quad (5)$$

Eq. (5) indicates the relationship between the degradation of scaffold element and the mechanical stimulation. Apparently, the mechanical stimulation increases the degradation rate of polymer.

### 2.3. Inclusion of autocatalysis into the stochastic hydrolysis

*In vitro* experiments have demonstrated that autocatalysis plays an important role in accelerating the local hydrolysis of polymers, and thus affects the polymer degradation (Lam et al., 2008). The mechanism of the autocatalysis is that long ester chains in polymers break into short chains with carboxyl end groups during hydrolysis, the carboxyl end groups catalyze the hydrolysis and increase the hydrolysis rate (Lam et al., 2008). As stated in (Arifin et al., 2006), the autocatalytic effect was induced by the high concentration of carboxyl end groups, which could not be timely diffused out of the polymer matrix. Thus, in order to include the autocatalytic effect into the above stochastic hydrolysis model, the diffusion of hydrolysates was considered.

Here, the autocatalysis includes three steps, *i.e.* the release, diffusion and catalysis of hydrolysates. To describe the release-diffusion process, we employ literature-defined concentration  $C_m$  of hydrolysates, and the concentration of all scaffold elements is set to zero before hydrolysis (*i.e.*,  $C_m = 0$  at  $t = 0$ ). When hydrolysis of a scaffold element starts, the hydrolysates are released. It is assumed that the polymer chain in the scaffold element is completely hydrolyzed as long as the size of the element is sufficiently small (Göpferich, 1997), and the autocatalysis has no effect on the degradation of the scaffold element when the hydrolysates are diffused out of the element. Then, the release-diffusion process of the hydrolysates in a scaffold element is modeled by Fick's

second law as (Thombre and Himmelstein, 1985):

$$\frac{\partial C_m}{\partial t} = \nabla(D_m \nabla C_m) + S(t) \tag{6}$$

where  $S(t)$  is a term denoting the source of hydrolysates in the element,  $D_m$  is the diffusion coefficient of hydrolysates, and experimental results showed that it could be empirically determined by the degree of degradation  $(1-\beta(t))$  (Thombre and Himmelstein, 1985), i.e.,

$$D_m = D_0 e^{\varphi(1-\beta(t))} \tag{7}$$

where  $D_0$  is the initial diffusion coefficient of non-hydrolyzed polymer,  $\varphi$  is a material-dependent constant.

It is stated that the autocatalysis related to the concentration of hydrolysates follows an exponential relationship compared to the hydrolysis without autocatalysis. Thus, we use an exponential function to model the autocatalysis as,

$$\lambda_a = \lambda_\sigma (e^{C_m} - 1) \tag{8}$$

where  $\lambda_a$  is the autocatalysis-included degradation rate of a scaffold element. Finally, considering the mechanical stimulation and autocatalysis, the resulting hydrolytic rate is expressed as

$$\lambda = \lambda_\sigma + \lambda_a = \lambda_0 e^{\frac{B\sigma}{RT}} e^{C_m} \tag{9}$$

Eq. (9) becomes Eq. (5) (or  $\lambda = \lambda_\sigma$ ) when the autocatalysis disappears (i.e.,  $C_m = 0$ ). Correspondingly, hybrid degradation formulations for a polymer scaffold element under the mechanical stimulation and autocatalysis are expressed as:

$$\begin{cases} \beta(t) = e^{-\lambda(t+t_{add})} \\ p(t) = k\lambda e^{-k\lambda(t+t_{add})} \end{cases} \tag{10}$$

### 2.4. Degradation judgment of scaffold element

Based on Eq. (10), we propose two degradation conditions: (1) The normalized number average molecular weight  $\beta(t)$  of each scaffold element decreases below a threshold  $\beta_{threshold}$ , the scaffold element is considered to be completely degraded; (2) The degradation probability  $\int_t^{t+dt} p(t)dt$  is less than a randomly generated number  $p$  from 0 to 1, the scaffold element is also considered to be completely degraded (Bose and Git, 2004; Shi et al., 2018). Under both conditions, the completely degraded element is changed into the immersing solution. Then, the criterion to judge the complete degradation of a scaffold element when either of the following conditions is satisfied,

$$\begin{cases} \beta(t) < \beta_{threshold} \\ \int_t^{t+dt} p(t)dt < p \end{cases} \tag{11}$$

The mechanical properties of polymers are related to their molecular weight (Nunes et al., 1982), and they decreases exponentially during degradation process (Blaker et al., 2011). The experimental result by Tsuji et al. (2015) shows that the downtrend is similar to exponential decrease of Young's modulus. Here, the Young's modulus  $E_s$  of the scaffold element is also exponentially related to its normalized number average molecular weight ratio before its complete degradation as (Shi et al., 2018):

$$E_s(t) = (E_s(0) - E_{solu}) \cdot \frac{e}{e-1} (1 - e^{-\beta(t)}) + E_{solu} \tag{12}$$

where  $E_s(0)$  is the initial Young's modulus of the scaffold element,  $E_{solu}$  is the Young's modulus of the solution, which is a constant during degradation process. For ideal scaffold elements, their initial porosity  $\alpha$  equals zero, we have  $t = 0$ ,  $t_{add} = 0$ ,  $\beta(0) = 1$ , and  $E_s(t) = E_s(0)$ . Whereas, completely degraded scaffold element has  $\beta(t) = 0$ , and  $E_s(t) = E_{solu}$ . Obviously, the two self-consistent conditions are satisfied. It is worth mentioning that we mainly take into account the mechanical stimulation and autocatalysis, and other factors (e.g. pH value,

crystallinity) are ignored in the model. However, the ignored factors indeed influence the degradation of the scaffold (Zolnik and Burgess, 2007; Tsuji et al., 2015).

### 2.5. Failure of degraded scaffold under mechanical stimulation

As polymer scaffold degrades, its strength decreases. If the scaffold-solution system cannot support the external applied load, the system collapses. Therefore, basing on average stresses of cross-sections of the system, we put forward a formula to calculate the average stresses to judge when the system collapses, i.e.,

$$\bar{\sigma}_i = \frac{\sum_{j=1}^{q_i(t)} \varepsilon_{s,crit} \times E_{s,j}(t) + \sum_{N_{layer}-q_i(t)}^{N_{layer}} \varepsilon_{solu} \times E_{solu}}{N_{layer}} \tag{13}$$

where  $\bar{\sigma}_i$  is the average stress acting on the  $i^{th}$ -layered system element,  $\varepsilon_{s,crit}$  is a constant critical strain of the scaffold element,  $\varepsilon_{solu}$  is the strain of the solution element,  $q_i(t)$  is a varying number of scaffold elements in the  $i$ th layer,  $E_{s,j}(t)$  is the Young's modulus of the  $j$ th scaffold element, and  $N_{layer}$  is the element number of each layer. It is worth mentioning that  $\varepsilon_{s,crit}$  is conservative, since  $\varepsilon_{s,crit}$  also decreases as a scaffold element degrades. Then, the calculated  $\bar{\sigma}_i$  is compared with the externally applied stress  $\sigma$ , and if any one of the layers is lower than  $\sigma$ , the system is considered to be collapsed, i.e.,

$$\bar{\sigma}_i < \sigma \tag{14}$$

## 3. Materials and methods

### 3.1. Materials

PLA is biodegradable, and has been approved by Food and Drug Administration (FDA), and used in many biomedical fields (Tyler et al., 2016; Mi et al., 2013, 2017). Thus, PLA was here considered as the constituent material of porous scaffolds, and the scaffolds were immersed in solutions like body fluid, which indicated that the pores of the scaffolds were initially occupied by the solutions. PLA was treated to be isotropic and linear-elastic, and its Young's modulus and Poisson's ratio were 5 GPa (Middleton and Tipton, 2000) and 0.3 (Shi et al., 2018), respectively. The solution was also treated to be isotropic and linear-elastic but in-compressive, and its Young's modulus was 10 MPa and Poisson's ratio 0.49 (Shi et al., 2018).

### 3.2. Scaffold structures and mesh

To investigate the effect of the mechanical stimulation on the degradation processes of different scaffold structures, three periodic scaffold structures named lattice, spherical and truss were designed. The lattice and spherical structures were already presented in (Adachi et al., 2006; Sanz-Herrera et al., 2009). Without loss of generality, their RVCs were treated like those in (Adachi et al., 2006; Sanz-Herrera et al., 2009), see upper row in Fig. 1. Geometrical sizes of the RVCs were shown in the middle row in Fig. 1. According to the geometrical parameters, their porosities were calculated as 64.8%, 67.8% and 64.5%, respectively, which complied with that of trabecular bone (Ding and Hvid, 2000). All the RVCs were uniformly divided into 8000 ( $20 \times 20 \times 20$ ) elements by a voxel element method, see the lower row in Fig. 1.

### 3.3. Boundary conditions

For each RVC, its bottom was fixed, and the load representing the mechanical stimulation was applied perpendicularly on its top to simulate the mechanical micro-environment in targeted sites, e.g. femoral shaft. To consider the influences of the surrounding RVCs and the host tissues, four lateral faces of the RVC were constrained to only allow the

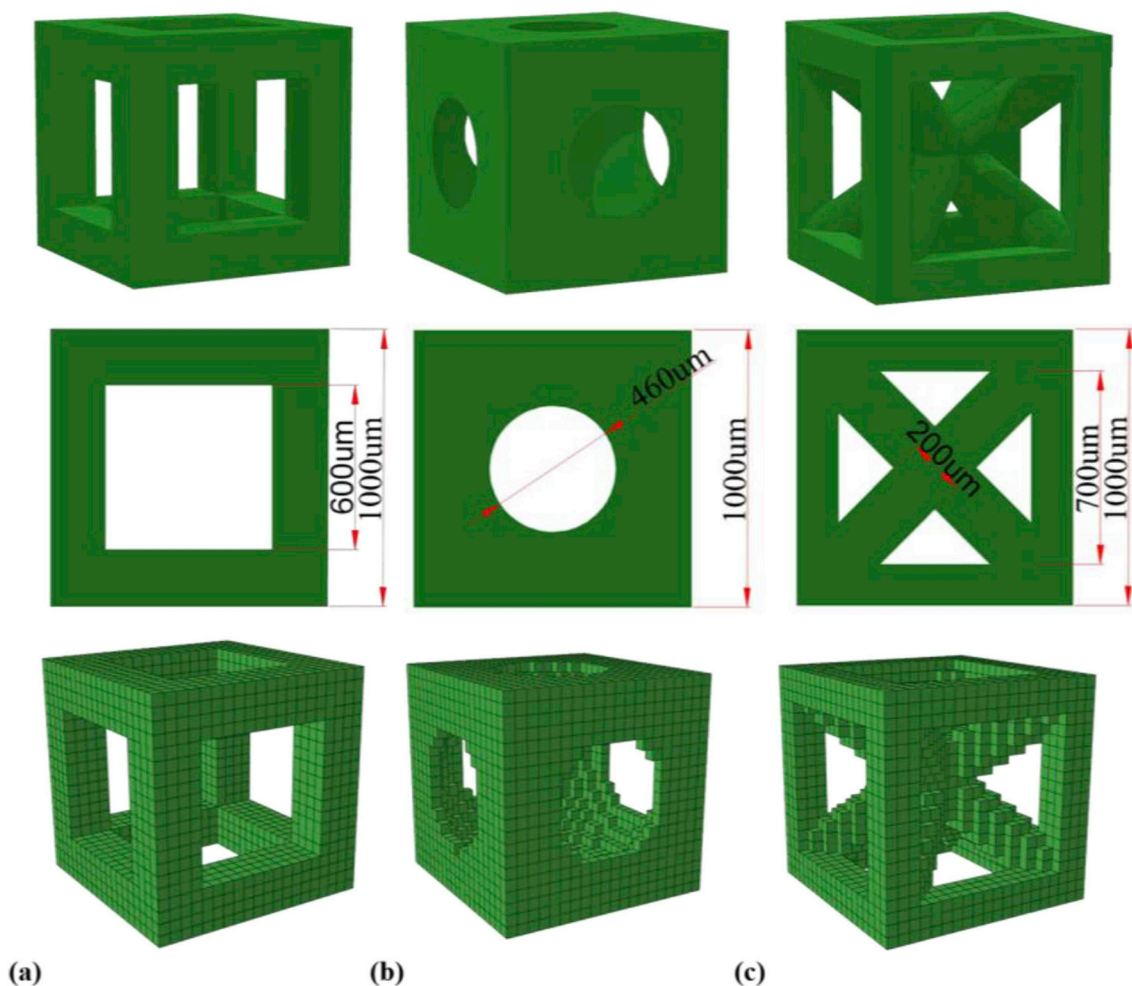


Fig. 1. Scaffold RVC structures and their geometric sizes. (a) Lattice, (b) spherical, and (c) truss RVCs.

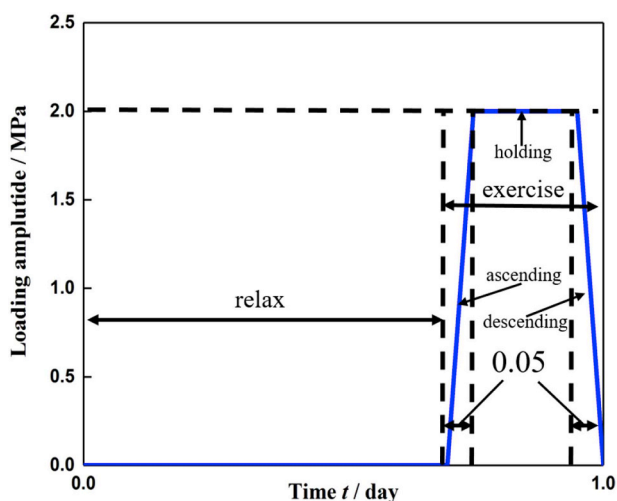


Fig. 2. Loading trapezoidal pulse in a day.

element nodes' to move in the loading direction. The loading history was periodic piecewise with the period 1 day, it involved an unloaded stage and a loaded stage including ascending, holding and descending sub-stages, as shown in Fig. 2. The two stages represented the rest and exercise activities of a patient in a day, respectively. It is noted that the ascending and descending stages were set to be 0.05 day to avoid the sudden change between the unloaded and loaded stages, which might

Table 1  
Input parameters of simulation.

Parameters	Value	Unit	
Degradation rate constant	$\lambda_0$	0.0075 (Li et al., 2017b)	day <sup>-1</sup>
Ratio	$k$	0.15	–
State change threshold	$\beta_{threshold}$	0.01 (Shi et al., 2018)	–
Constant	$B$	22 (Li et al., 2017b)	J/(mol·Pa)
Gas constant	$R$	8.314	J/(mol·K)
Temperature	$T$	310	K
Initial diffusion coefficient in polymer	$D_0$	$1.2 \times 10^{-9}$ (Gleadall et al., 2014)	m <sup>2</sup> /day
Material constant for diffusivity	$\varphi$	9.43 (Gleadall et al., 2014)	–
Young's modulus of scaffold	$E_s$	5 (Middleton and Tipton, 2000)	GPa
Young's modulus of solution	$E_{solu}$	0.01 (Shi et al., 2018)	GPa
Poisson's ratio of scaffold	$\nu_s$	0.3 (Shi et al., 2018)	–
Poisson's ratio of solution	$\nu_{ECM}$	0.49 (Shi et al., 2018)	–
Critical strain of scaffold	$\epsilon_{s,crit}$	5% (Nishida et al., 2009)	–
Critical strain of solution	$\epsilon_{solu}$	5%	–

induce the inconvergence in the simulation.

### 3.4. Numerical implementation

The loading stress on human bones is ranging from 0.2 MPa to 4.0 MPa during normal walking (Urban, 1994). Here, the loading intensities were 1.0 MPa, 1.5 MPa and 2.0 MPa, and the loading durations were 0.1, 0.2 and 0.3 day per day. Thus, nine cases with the above

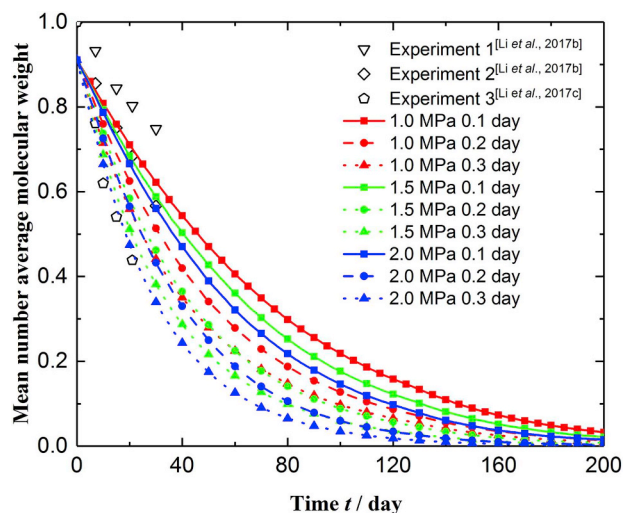


**Fig. 3.** Comparison of the mean number average molecular weight between the simulation of the lattice scaffold and *in vitro* degradation experiments. Experiment 1: Degradation of neat-PLA immersed in Kirkland's biocorrosion media (KBM) with pH value 7.4 at 37 °C under no mechanical stimulation (Li et al., 2017b); experiment 2: Degradation of neat-PLA immersed in Kirkland's biocorrosion media (KBM) with pH value 7.4 at 37 °C under loading intensity 1.0 MPa (Li et al., 2017b); experiment 3: Degradation of neat-PLA immersed in Kirkland's biocorrosion media (KBM) with pH value 7.4 at 37 °C under 0.9 MPa loading intensity at 1.0 Hz (Li et al., 2017c).

loading intensities and durations for each RVC were treated (27 models for the three RVCs). The dynamic degradation process was simulated by using Abaqus/Explicit (*DS SIMULIA*, USA) and coding user subroutine (VUMAT). To solve the nonlinear models efficiently, Abaqus/Explicit was employed here to guarantee the calculation convergence compared to Abaqus/Standard, and an auto-incremental step was adopted. All the

input parameters in the simulations are listed in Table 1.

### 3.5. Sensitivity analysis

The sensitivity analysis was also performed by varying four key parameters in Table 1, i.e., degradation rate constant  $\lambda_0$ , state change threshold  $\beta_{\text{threshold}}$ , initial diffusion coefficient  $D_0$  in polymer and Young's modulus  $E_s$  of scaffold constituent material. This is because the four parameters are directly related to the degradation speed, judgment of complete degradation, autocatalysis, and selection of scaffold constituent materials. On the basis of the input values of the four parameters in Table 1, we fluctuated them by plus and minus 20%, and additional 216 models were simulated to study their sensitivity on the degradation of the scaffolds. The sensitivity index  $S$  was defined as,

$$S = \left| \frac{\Delta Y_i}{\Delta X_i} \right| = \left| \frac{Y_i(X_i + \omega X_i) - Y_i(X_i - \omega X_i)}{2\omega X_i} \right| \quad (15)$$

where  $X_i = \lambda_0, \beta_{\text{threshold}}, D_0, E_s$  are input variables,  $Y_i$  is a output variable, and  $\omega = 20\%$  is the fluctuation of the four input variables.

## 4. Results and discussions

### 4.1. Model validation and the scaffold degradation process

To validate the proposed model, we compared the simulated mean number average molecular weight  $\beta(t)$  of all residual scaffold elements in the lattice scaffold with experimental data (Li et al., 2017b, 2017c) in Fig. 3. Here,  $\beta(t)$  of the scaffolds was calculated through dividing the sum of  $\beta(t)$  of all the residual scaffold elements by the number of the initial scaffold elements. Generally, Fig. 3 shows that the downward tendency of  $\beta(t)$  before day 30 is comparable to the literature although there exists slight deviation of experimental conditions (Li et al., 2017b, 2017c). In experiment 1, PLA received no mechanical stimulation, its mean number average molecular weight decreases slower than others;

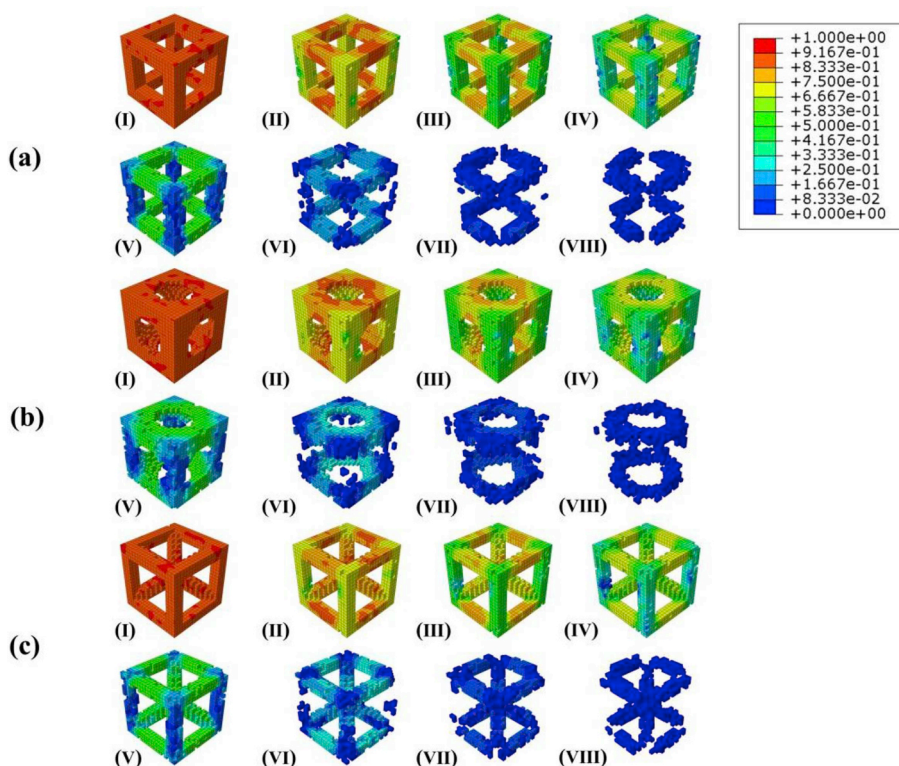


**Fig. 4.** The evolution of  $\beta(t)$  of the three RVCs within 200 days (a) Lattice, (b) spherical, and (c) truss structures. (I. day 1, II. day 10, III. day 20, IV. day 30, V. day 50, VI. day 100, VII. day 150, VIII. day 200).

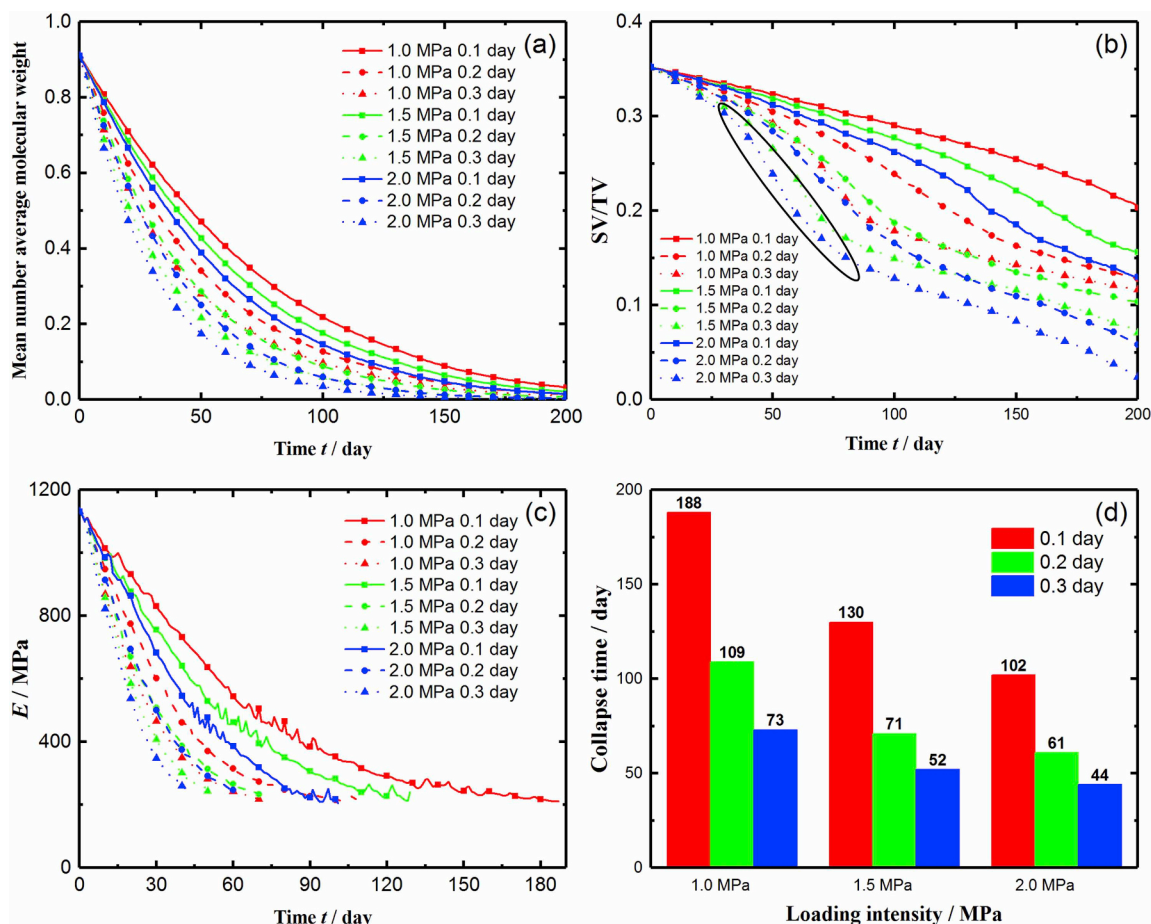


Fig. 5. Degradation of the nine cases of the lattice structure: (a)  $\bar{\beta}(t)$ ; (b) SV/TV; (c) Young's modulus of scaffold-solution system; (d) collapsing time of the system.

in experiment 2, PLA received 1.0 MPa loading intensity, it is comparable to the present 1.0 MPa simulation; in experiment 3, PLA received 0.9 MPa loading intensity at 1 Hz loading frequency, despite of the lower loading intensity, the mean number average molecular weight decrease at a faster rate than others because of the influence of the loading frequency. Moreover, by using Eq. (1), the inversely calculated average degradation rate within the first 30 days was  $2.17 \times 10^{-2}/\text{day}$ , which is in the same order as the degradation rates  $5.08 \times 10^{-2}/\text{day}$  (Tsuji et al., 2011) and  $4 \times 10^{-2}/\text{day}$  (Helder et al., 1990), respectively. In any case, these findings demonstrate a relatively quantitative validation of the proposed model.

To illustrate the degradation process of the three RVCs, a specific case with the loading intensity 1.5 MPa and duration 0.2 day was presented. During their degradation processes,  $\beta(t)$  at eight time points were snapshot and shown in Fig. 4. The four pillars of the three RVCs along the loading direction degraded at a faster rate than the horizontal or inclined pillars because of the higher stress. This indicates that the mechanical stimulation promotes polymer degradation. In particular, before day 50 (time point V), the vertical pillars were not completely degraded, whereas the vertical pillars were completely degraded after day 150 (time point VII).

#### 4.2. Effect of mechanical stimulation on the three scaffolds

For the lattice structure, its degradation properties influenced by the mechanical stimulation are shown in Fig. 5. Generally, it shows that the nine cases with different mechanical stimulations shared a trend that scaffold degraded quickly during early period. For a loading duration, the higher loading intensity, the more  $\bar{\beta}(t)$  decreases; while for a loading intensity, the longer loading duration, the more  $\bar{\beta}(t)$  reduces, as

shown in Fig. 5a. The varying volume fraction (SV/TV, SV is the volume of residual scaffold elements, and TV is the sum of the volumes of scaffold and solution elements) of the residual scaffold element is shown in Fig. 5b. Different from  $\bar{\beta}(t)$ , SV/TV gently decreased during degradation. For example, in the case of the loading intensity 2.0 MPa at day 50,  $\bar{\beta}(t)$  was about 0.40, 0.26, and 0.18 for the duration 0.1 day, 0.2 day and 0.3 day, respectively; correspondingly, SV/TV was 88.81%, 81.53% and 69.03%. This indicates that the scaffold elements were not completely degraded even though their number average molecular weight greatly decreased. Plus, increases in both loading intensity and duration greatly reduced SV/TV, e.g. the circled part between day 25 and day 75 for the loading intensity 2.0 MPa and duration 0.3 day in Fig. 5b. The Young's modulus of the scaffold-solution system is shown in Fig. 5c. It is worth mentioning that the Young's modulus before the system collapse was only calculated on the basis of losing supporting ability to the external stress. Complying with  $\bar{\beta}(t)$  and SV/TV, the Young's modulus also decreased more with a higher loading intensity or a longer loading duration, and approached to a final modulus around  $225.86 \pm 20.36$  MPa. The collapse time of the scaffold-solution system is presented in Fig. 5d, and a greater loading intensity or duration resulted in an earlier system collapse.

For the spherical structure, its degradation properties influenced by the mechanical stimulation are shown in Fig. 6. Like the lattice structure,  $\bar{\beta}(t)$ , SV/TV, Young's modulus, and the collapse time were influenced by the loading intensity and duration. Namely, an increase in the loading intensity and duration accelerated the spherical scaffold degradation. However, the final Young's modulus of the nine cases was  $246.09 \pm 28.75$  MPa, which was greater than that of the lattice structure  $225.86 \pm 20.36$  MPa. Moreover, their collapse time was  $102 \pm 63$  day, which was smaller than those of the lattice structure

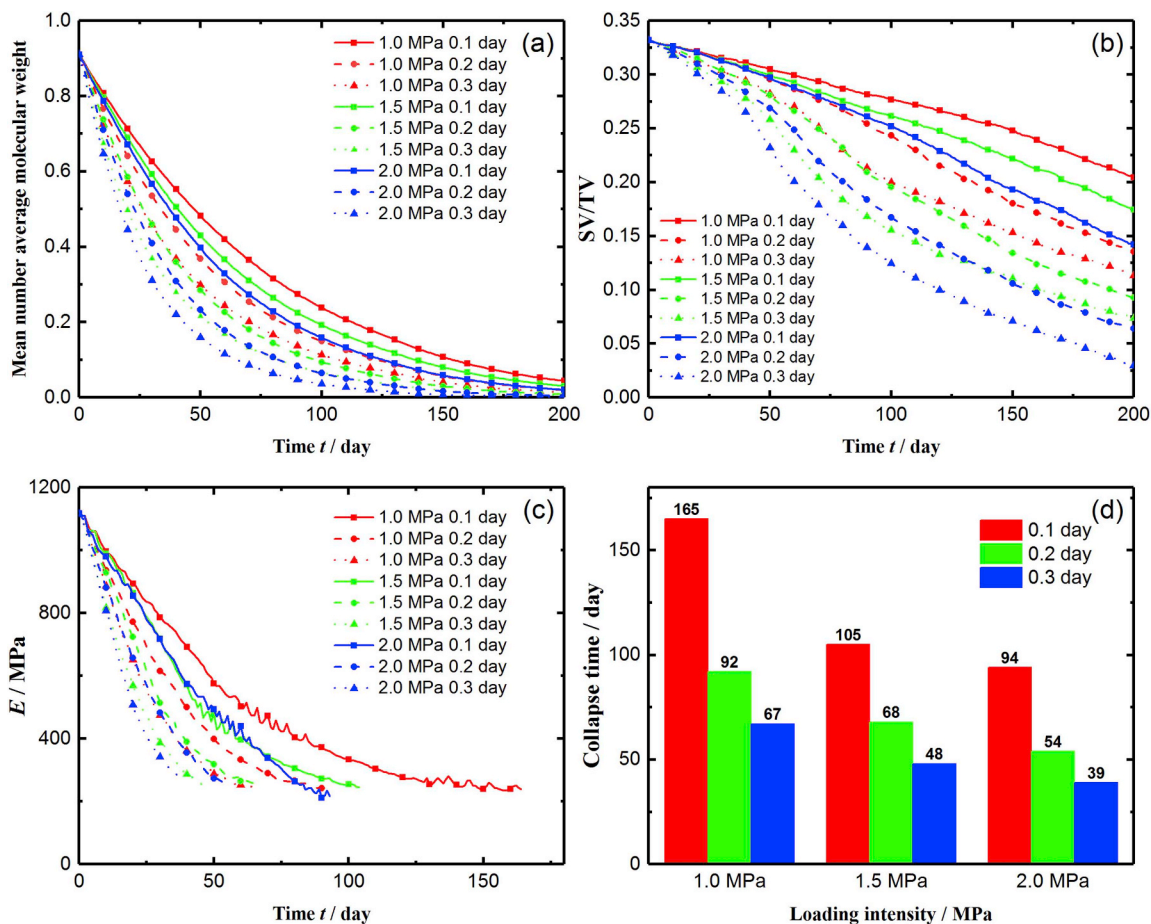


Fig. 6. Degradation of the nine cases of the spherical structure: (a)  $\bar{\beta}(t)$ ; (b) SV/TV; (c) Young's modulus of scaffold-solution system; (d) collapsing time of the system.

(116 ± 72 day).

For the truss structure, its degradation properties influenced by the mechanical stimulation are shown in Fig. 7. Again, like the lattice and spherical structures,  $\bar{\beta}(t)$ , SV/TV, Young's modulus, and the collapse time were influenced by the loading intensity and duration. The increase in the loading intensity and duration speeded up the truss scaffold degradation. In particular, the final Young's modulus of the nine cases was 202.03 ± 13.67 MPa, which was smaller than that of either the lattice structure (225.86 ± 20.36 MPa) or the spherical structure (246.09 ± 28.75 MPa). However, the truss structure collapsed later than the above two structures. In particular, for the loading intensity 1.0 MPa with durations 0.1 day and 0.2 day, the structure did not collapse within the 200 days.

In all, for the three structures, these results indicate that a greater loading intensity or duration is beneficial for the scaffold degradation. The result is consistent with the experiments (Li et al., 2017c; Yang et al., 2008; Smutz et al., 1991; Tong and White, 1996). In the sense of degradation mechanism, the mechanical stimulation decreases the activation energy of polymer hydrolysis (Eqs. (4) and (5)), which accelerates the scaffold degradation. However, Kang et al. (2007) found that the mass loss rate of porous poly(L-lactic acid)/β-tricalcium phosphate composite scaffold under the static compression was slower than that of non-loading case. The inconsistency with the literature might be attributed to retarded penetration of simulated body fluid into the scaffold, which depressed the hydrolysis of the polymer component in the composite scaffold.

#### 4.3. Comparison of the three structures

To illustrate different degradations of the three structures, we only

compared their results of the specific case with the loading intensity of 2.0 MPa and the duration of 0.1 day, and the comparison is shown in Fig. 8. Generally, different scaffold structures weakly influence  $\bar{\beta}(t)$ , SV/TV, Young's modulus, but apparently influence the collapse time. Particularly,  $\bar{\beta}(t)$  is in the order truss > spherical > lattice (Fig. 8a). SV/TV represents the percentage of the residual scaffold elements in structures. In other words, the number of the residual scaffold elements in the truss structure is greater than the other two (Fig. 8b). Moreover, with the similar porosities (64.8% for the lattice structure and 64.5% for the truss structure), the truss structure degrades more slowly due to the shared load by oblique pillars (see Fig. 9a,c), and better diffusion ability of hydrolysates, which mitigates the autocatalytic effect (see Fig. 9d,f). The number of the residual scaffold element in the spherical structure is smallest, and this is due to the greatest initial porosity (67.8%), but its degradation mode is similar to that of the truss structure. The Young's moduli of the lattice and spherical structures share a decreasing tendency, which is above that of the truss structure before day 70 but below that after day 70 (Fig. 8c). This is because the truss structure is more compliant due to the existence of the oblique pillars, which is mainly bent instead of axial loaded under the external stress. After day 70, due to its slow degradation (Fig. 8a and b), the Young's modulus of the truss structure is greater than the other two. As for the collapse times, they are in the order of truss > lattice > spherical (Fig. 8d). The reason is that the truss structure under the external stress is more stable than the other two due to the oblique pillars (Fig. 9c), and the spherical structure has the weakest middle cross-section which makes the system collapse earlier (Fig. 9b).

It is worth mentioning that the internal surface areas of the lattice, spherical, and truss structures approximately were calculated as 2.88 mm<sup>2</sup>, 2.76 mm<sup>2</sup>, 6.36 mm<sup>2</sup>, respectively, thus, it seems

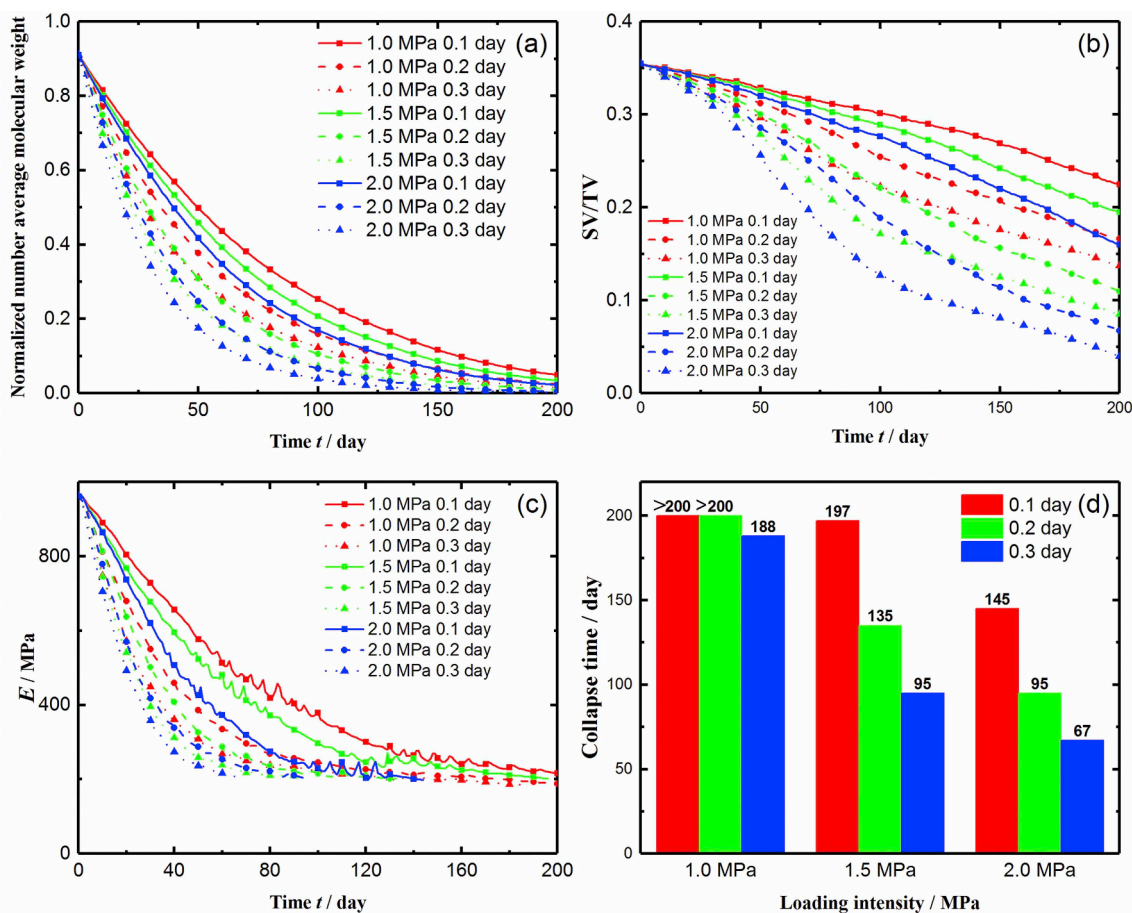


Fig. 7. Degradation of the nine cases of the truss structure: (a)  $\bar{\beta}(t)$ ; (b) SV/TV; (c) Young's modulus of scaffold-solution system; (d) collapsing time of the system.

contradictory to our intuition that the truss structure with the highest surface area should degrade faster than the other two structures. In this regard, we here consider the bulk erosion instead of surface erosion since the critical size judging bulk or surface degradations of ester polymer is greater the pillar thickness of the present structures (Han and Pan, 2009), so the bulk degradation of scaffold dominate. Moreover, the mechanical stimulation and the diffusion-governed autocatalysis in the bulk degradation of all scaffold elements is the same in theory (Eq. (9)), and for the truss structure, the external stress is shared by the oblique pillars and has a better diffusion ability to mitigate the autocatalytic effect. Therefore, the truss structure degrades most slowly, see Fig. 9c.

#### 4.4. Sensitivity analysis

All the results of the additional 216 models in sensitivity analysis are reported in Supporting Materials. Because the mean number average molecular weight, SV/TV, and Young's modulus are varying in the degradation process, we only analyzed the sensitivity by the collapse time ( $Y_c$ ). Plus, in view of the huge amount of results, a specific case with the loading intensity 1.5 MPa and duration 0.2 day of the three structures were discussed. According to Eq. (15), the sensitivity index  $S$  are shown in Table 2. Apparently, the sensitivities of the four parameters are in the order of  $D_0 > \lambda_0 > \beta_{\text{threshold}} > E_s$ . This indicates that a very weak fluctuation of  $D_0$  can result in a great variation of the collapse time.

#### 4.5. Limitations

Indeed, there are limitations. Other factors, such as crystallization

and loading frequency should be included. The crystallization (Tsuji et al., 2015) and loading frequency (Li et al., 2017c) influence the polymer degradation, but these issues are here ignored. Second, the collapse time is calculated conservatively: on the one hand, the critical strain of scaffold element in Eq. (13) is constant. On the other hand, the solution is treated as an in-compressive solid material which retarded the collapse time. Third, the numerical result has not been fully validated through experiments which will be treated in the near future.

## 5. Conclusions

We developed a mathematical model to study the dynamic degradation processes of three porous scaffolds under different mechanical stimulations by including the mechanical and autocatalytic effects. The results showed that the mechanical stimulation accelerated the degradation of the PLA scaffolds. However, the degradation of the three structures with a similar porosity was weakly influenced by the mechanical stimulations except for their collapse times. Importantly, the initial diffusion coefficient was very sensitive to the collapse time induced by the scaffold degradation. The present work improves our understanding of polymer degradation and could be helpful for future design of suitable biodegradable scaffolds for tissue engineering.

## Acknowledgements

This study was supported by the National Natural Science Foundation of China (NSFC) (No. 31300780, 61821002, 11772093), the Fundamental Research Funds for the Central Universities (No. 2242016R30014), and partially supported by the National 973 Basic Research Program of China (No. 2013CB733800) and ARC

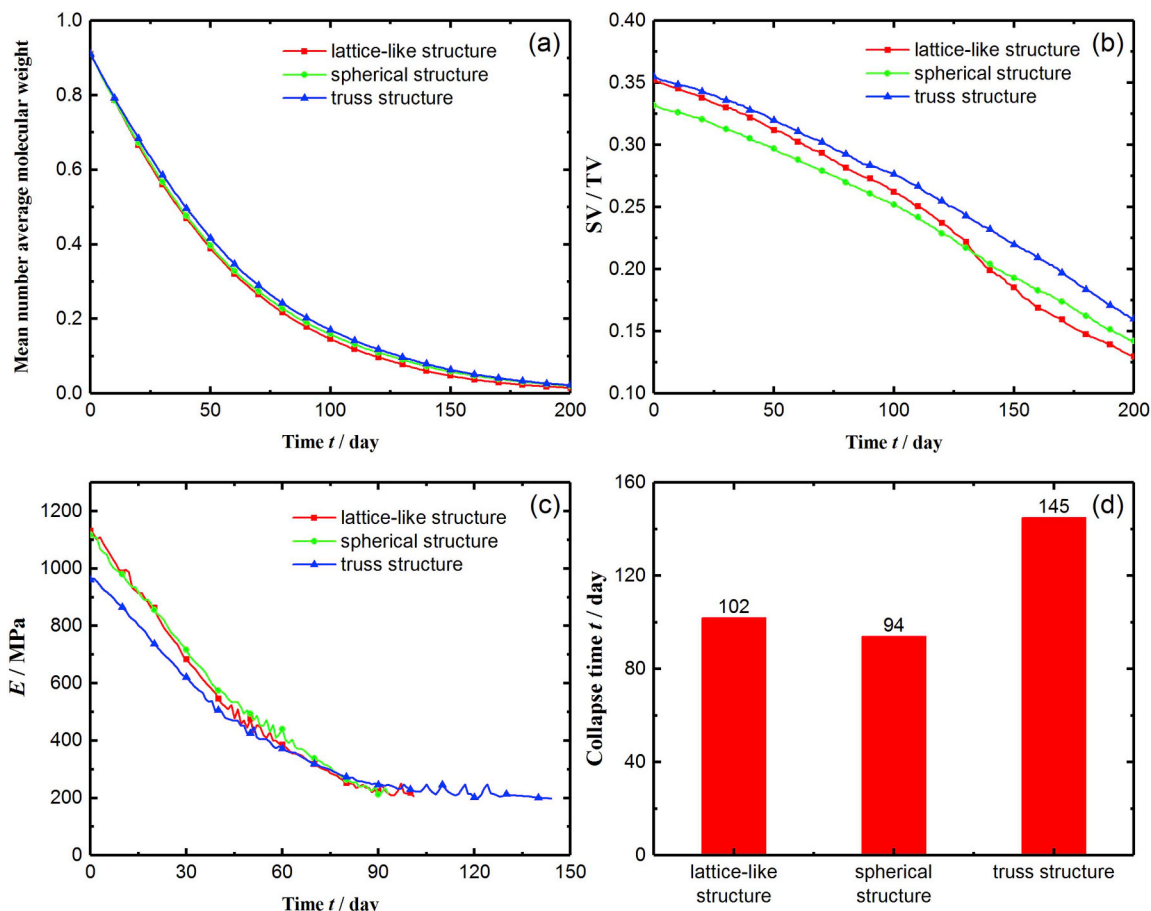


Fig. 8. Comparison of the three structures with loading intensity of 2.0 MPa and duration of 0.1 day: (a)  $\bar{\beta}(t)$ ; (b) SV/TV; (c) Young's modulus; (d) collapsing time.

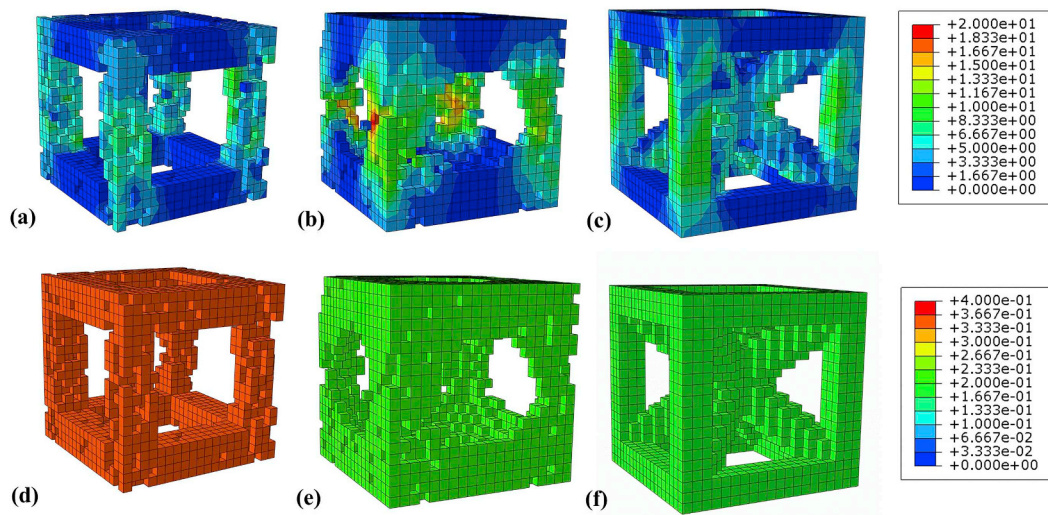


Fig. 9. Stress and  $C_m$  in the residual elements of the three structures with the loading intensity of 2.0 MPa and the duration of 0.1 day at day 50. Stresses of lattice (a), spherical (b), truss (c), and  $C_m$  of lattice (d), spherical (e), truss (f).

Table 2  
Sensitivity index  $S$  of the collapse time ( $Y_i$ ).

$X_i$	$\lambda_0$	$\beta_{\text{threshold}}$	$D_0$	$E_s$
Lattice	$8.0 \times 10^3$	$5.0 \times 10^2$	0.0	1.5
Spherical	$9.7 \times 10^3$	0.0	$4.2 \times 10^9$	2.5
Truss	$1.4 \times 10^4$	$4.3 \times 10^3$	$4.2 \times 10^{10}$	10.5

(FT140101152). NMP is supported by the European Commission with the Graphene Flagship Core 2 n. 785219 (WP14 “Composites”) and FET Proactive “Neurofibres” n. 732344 as well as by the MIUR with the “Departments of Excellence” grant L. 232/2016 and ARS01-01384-PROSCAN.

## Appendix A. Supplementary data

Supplementary data related to this article can be found at <https://doi.org/10.1016/j.jmbbm.2019.04.028>.

## References

- Adachi, T., Osako, Y., Tanaka, M., et al., 2006. Framework for optimal design of porous scaffold microstructure by computational simulation of bone regeneration. *Biomaterials* 27 (21), 3964–3972.
- Antheunis, H., van der Meer, J.C., de Geus, M., et al., 2010. Autocatalytic equation describing the change in molecular weight during hydrolytic degradation of aliphatic polyesters. *Biomacromolecules* 11 (4), 1118–1124.
- Arifin, D.Y., Lee, L.Y., Wang, C.H., 2006. Mathematical modeling and simulation of drug release from microspheres: implications to drug delivery systems. *Adv. Drug Deliv. Rev.* 58 (12–13), 1274–1325.
- Blaker, J.J., Nazhat, S.N., Maquet, V., et al., 2011. Long-term in vitro degradation of PDLA/Bioglass® bone scaffolds in acellular simulated body fluid. *Acta Biomater.* 7 (2), 829–840.
- Bose, S.M., Git, Y., 2004. Mathematical modelling and computer simulation of linear polymer degradation: simple scissions. *Macromol. Theory Simul.* 13 (5), 453–473.
- Chen, Y., Zhou, S., Li, Q., 2011. Mathematical modeling of degradation for bulk-erosive polymers: applications in tissue engineering scaffolds and drug delivery systems. *Acta Biomater.* 7 (3), 1140–1149.
- Ding, M., Hvid, I., 2000. Quantification of age-related changes in the structure model type and trabecular thickness of human tibial cancellous bone. *Bone* 26 (3), 291–295.
- Fan, Y.B., Li, P., Zeng, L., et al., 2008. Effects of mechanical load on degradation of poly (D,L-lactic acid) foam. *Polym. Degrad. Stabil.* 93 (3), 677–683.
- Gleadall, A., Pan, J., Kruff, M.A., et al., 2014. Degradation mechanisms of bioresorbable polyesters. Part 1. Effects of random scission, end scission and autocatalysis. *Acta Biomater.* 10 (5), 2223–2232.
- Gómez, S., Vlad, M.D., López, J., et al., 2016. Design and properties of 3D scaffolds for bone tissue engineering. *Acta Biomater.* 42, 341–350.
- Göpferich, A., 1996. Mechanisms of polymer degradation and erosion. *Biomaterials* 17 (2), 103–114.
- Göpferich, A., 1997. Polymer bulk erosion. *Macromolecules* 30 (9), 2598–2604.
- Göpferich, A., Langer, R., 1993. Modeling of polymer erosion. *Macromolecules* 26 (16), 4105–4112.
- Han, X., Pan, J., 2009. A model for simultaneous crystallisation and biodegradation of biodegradable polymers. *Biomaterials* 30 (3), 423–430.
- Helder, J., Dijkstra, P.J., Feijen, J., 1990. In vitro degradation of glycine/DL-lactic acid copolymers. *J. Biomed. Mater. Res.* A 24 (8), 1005–1020.
- Hutmacher, D.W., 2000. Scaffolds in tissue engineering bone and cartilage. *Biomaterials* 21 (24), 2529–2543.
- Kang, Y.Q., Yin, G.F., Luo, L., et al., 2007. Effects of mechanical stress on the in vitro degradation of porous composite scaffold for bone tissue engineering. *Key Eng. Mater.* 342, 273–276.
- Kang, Y., Yao, Y., Yin, G., et al., 2009. A study on the in vitro degradation properties of poly (l-lactic acid)/ $\beta$ -tricalcium phosphate (PLLA/ $\beta$ -TCP) scaffold under dynamic loading. *Med. Eng. Phys.* 31 (5), 589–594.
- Lam, C.X.F., Savalani, M.M., Teoh, S.H., et al., 2008. Dynamics of in vitro polymer degradation of polycaprolactone-based scaffolds: accelerated versus simulated physiological conditions. *Biomed. Mater.* 3 (3), 034108.
- Li, Y., Chu, Z., Li, X., et al., 2017a. The effect of mechanical loads on the degradation of aliphatic biodegradable polyesters. *Regen. Biomater.* 4 (3), 179–190.
- Li, X., Chu, C., Wei, Y., et al., 2017b. In vitro degradation kinetics of pure PLA and Mg/PLA composite: effects of immersion temperature and compression stress. *Acta Biomater.* 48, 468–478.
- Li, X., Qi, C., Han, L., et al., 2017c. Influence of dynamic compressive loading on the in vitro degradation behavior of pure PLA and Mg/PLA composite. *Acta Biomater.* 64, 269–278.
- Mi, H.Y., Salick, M.R., Jing, X., et al., 2013. Characterization of thermoplastic polyurethane/poly(lactic acid) (TPU/PLA) tissue engineering scaffolds fabricated by microcellular injection molding. *Mater. Sci. Eng. C* 33 (8), 4767–4776.
- Mi, H.Y., Jing, X., Turg, L.S., 2015. Fabrication of porous synthetic polymer scaffolds for tissue engineering. *J. Cell. Plast.* 51 (2), 165–196.
- Mi, H.Y., Jing, X., Napiwocki, B.N., et al., 2017. Biocompatible, degradable thermoplastic polyurethane based on polycaprolactone-block-polytetrahydrofuran-block-polycaprolactone copolymers for soft tissue engineering. *J. Mater. Chem. B* 5 (22), 4137–4151.
- Mi, H.Y., Jing, X., Yilmaz, G., et al., 2018. In situ synthesis of polyurethane scaffolds with tunable properties by controlled crosslinking of tri-block copolymer and polycaprolactone triol for tissue regeneration. *Chem. Eng. J.* 348, 786–798.
- Middleton, J.C., Tipton, A.J., 2000. Synthetic biodegradable polymers as orthopedic devices. *Biomaterials* 21 (23), 2335–2346.
- Nicodemus, G.D., Shipton, K.A., Kaltz, S.R., et al., 2009. Dynamic compressive loading influences degradation behavior of PEG-PLA hydrogels. *Biotechnol. Bioeng.* 102 (3), 948–959.
- Nishida, M., Yamaguchi, M., Todo, M., et al., 2009. Evaluation of dynamic compressive properties of PLA polymer blends using split Hopkinson pressure bar. In: *International Conference on the Mechanical and Physical Behaviour of Materials Under Dynamic Loading* 1. pp. 909–915.
- Nunes, R.W., Martin, J.R., Johnson, J.F., 1982. Influence of molecular weight and molecular weight distribution on mechanical properties of polymers. *Polym. Eng. Sci.* 22 (4), 205–228.
- Rose, F.R.A.J., Oreffo, R.O.C., 2002. Bone tissue engineering: hope vs hype. *Biochem. Biophys. Res. Commun.* 292 (1), 1–7.
- Sackett, C.K., Narasimhan, B., 2011. Mathematical modeling of polymer erosion: consequences for drug delivery. *Int. J. Pharm.* 418 (1), 104–114.
- Sanz-Herrera, J.A., Garcia-Aznar, J.M., Doblaré, M., 2009. On scaffold designing for bone regeneration: a computational multiscale approach. *Acta Biomater.* 5 (1), 219–229.
- Shi, Q., Chen, Q., Pugno, N., et al., 2018. Effect of rehabilitation exercise durations on the dynamic bone repair process by coupling polymer scaffold degradation and bone formation. *Biomechanics Model. Mechanobiol.* 17 (3), 763–775.
- Siepmann, J., Elkharraz, K., Siepmann, F., et al., 2005. How autocatalysis accelerates drug release from PLGA-based microparticles: a quantitative treatment. *Biomacromolecules* 6 (4), 2312–2319.
- Siparsky, G.L., Voorhees, K.J., Miao, F., 1998. Hydrolysis of polylactic acid (PLA) and polycaprolactone (PCL) in aqueous acetonitrile solutions: autocatalysis. *J. Environ. Polym. Degrad.* 6 (1), 31–41.
- Smutz, W.P., Daniels, A.U., Andriano, K.P., et al., 1991. Mechanical test methodology for environmental exposure testing of biodegradable polymers. *J. Appl. Biomater.* 2 (1), 13–22.
- Su, Y., Champagne, S., Trenggono, A., et al., 2018. Development and characterization of silver containing calcium phosphate coatings on pure iron foam intended for bone scaffold applications. *Mater. Des.* 148, 124–134.
- Thombre, A.G., Himmelstein, K.J., 1985. A simultaneous transport-reaction model for controlled drug delivery from catalyzed bioerodible polymer matrices. *AIChE J.* 31 (5), 759–766.
- Thompson, D.E., Agrawal, C.M., Athanasiou, K., 1996. The effects of dynamic compressive loading on biodegradable implants of 50–50% polylactic acid–polyglycolic acid. *Tissue Eng.* 2 (1), 61–74.
- Tong, L., White, J.R., 1996. Photo-oxidation of thermoplastics in bending and in uniaxial compression. *Polym. Degrad. Stabil.* 53 (3), 381–396.
- Tsuji, H., Eto, T., Sakamoto, Y., 2011. Synthesis and hydrolytic degradation of substituted poly (DL-Lactic Acid)s. *Materials* 4 (8), 1384–1398.
- Tsuji, H., Mizuno, A., Ikada, Y., 2015. Properties and morphology of poly(L-lactide). III. Effects of initial crystallinity on long-term in vitro hydrolysis of high molecular weight poly(L-lactide) film in phosphate-buffered solution. *J. Appl. Polym. Sci.* 77 (7), 1452–1464.
- Tyler, B., Gullotti, D., Mangraviti, A., et al., 2016. Polylactic acid (PLA) controlled delivery carriers for biomedical applications. *Adv. Drug Deliv. Rev.* 107, 163–175.
- Urban, J.P.G., 1994. The chondrocyte: a cell under pressure. *Rheumatology* 33 (10), 901–908.
- von Burkersroda, F., Schedl, L., Göpferich, A., 2002. Why degradable polymers undergo surface erosion or bulk erosion. *Biomaterials* 23 (21), 4221–4231.
- Wu, L., Ding, J., 2010. Effects of porosity and pore size on in vitro degradation of three-dimensional porous poly(D,L-lactide-co-glycolide) scaffolds for tissue engineering. *J. Biomed. Mater. Res. A* 75A (4), 767–777.
- Yang, Y., Zhao, Y., Tang, G., et al., 2008. In vitro degradation of porous poly (l-lactide-co-glycolide)/ $\beta$ -tricalcium phosphate (PLGA/ $\beta$ -TCP) scaffolds under dynamic and static conditions. *Polym. Degrad. Stabil.* 93 (10), 1838–1845.
- Zhang, R., Ma, P.X., 1999. Poly ( $\alpha$ -hydroxyl acids)/hydroxyapatite porous composites for bone-tissue engineering. I. Preparation and morphology. *J. Biomed. Mater. Res.* 44 (4), 446–455.
- Zhang, Q., Jiang, Y., Zhang, Y., et al., 2013. Effect of porosity on long-term degradation of poly ( $\epsilon$ -caprolactone) scaffolds and their cellular response. *Polym. Degrad. Stabil.* 98 (1), 209–218.
- Zhang, T., Zhou, S., Gao, X., et al., 2017. A multi-scale method for modeling degradation of bioresorbable polyesters. *Acta Biomater.* 50, 462–475.
- Zhurkov, S.N., Korsukov, V.E., 1974. Atomic mechanism of fracture of solid polymers. *J. Polym. Sci. Polym. Phys. Ed* 12 (2), 385–398.
- Zolnik, B.S., Burgess, D.J., 2007. Effect of acidic pH on PLGA microsphere degradation and release. *J. Control. Release* 122 (3), 338–344.

## Supporting Materials

### Effect of mechanical stimulation on the degradation of poly(lactic acid)scaffolds with different designed structures

Hengtao Shui<sup>1</sup>, Quan Shi<sup>1</sup>, Nicola Pugno<sup>2,3,4</sup>, Qiang Chen<sup>1,\*</sup>, Zhiyong Li<sup>1,5\*</sup>

<sup>1</sup>*Biomechanics Laboratory, School of Biological Science & Medical Engineering, Southeast University, 210096, Nanjing, P.R. China*

<sup>2</sup>*Laboratory of Bio-Inspired & Graphene Nanomechanics, Department of Civil, Environmental and Mechanical Engineering, University of Trento, I-38123 Trento, Italy.*

<sup>3</sup>*School of Engineering and Materials Science, Queen Mary University of London, Mile End Road E14NS, London, UK*

<sup>4</sup>*Ket Lab, Edoardo Amaldi Foundation, Italian Space Agency, Via del Politecnico snc, I-1100133 Rome*

<sup>5</sup>*School of Chemistry, Physics and Mechanical Engineering, Queensland University of Technology (QUT), Brisbane, QLD 4001, Australia*

### Sensitivity analysis

The sensitivity analysis was performed by varying the following four key parameters in the degradation model by plus and minus 20% fluctuation for the three presented structures (216 models), i.e., degradation rate constant  $\lambda_0$ , state change threshold  $\beta_{\text{threshold}}$ , initial diffusion coefficient in polymer  $D_0$  and Young's modulus of scaffold  $E_s$ . This is because the four parameters directly influence the degradation speed, judgment of complete degradation, autocatalytic effect, and materials selection of scaffold elements. All the results of the treated models are presented in the following figures.

### The lattice structures

$\lambda_0$  down-regulated by 20%

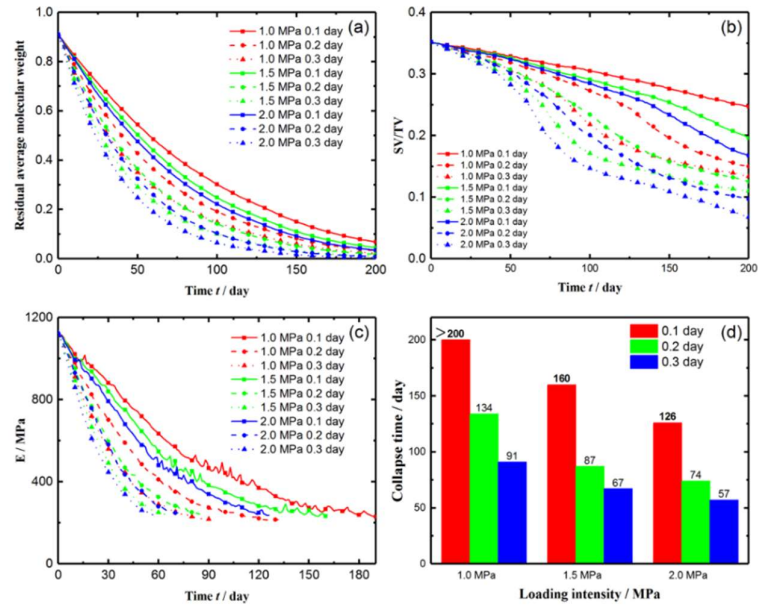


Fig. S1. Degradation of the nine cases of the lattice structure: (a)  $\bar{\beta}(t)$ ; (b) SV/TV; (c) Young's modulus of scaffold-solution system; (d) collapsing time of the system.

$\lambda_0$  up-regulated by 20%

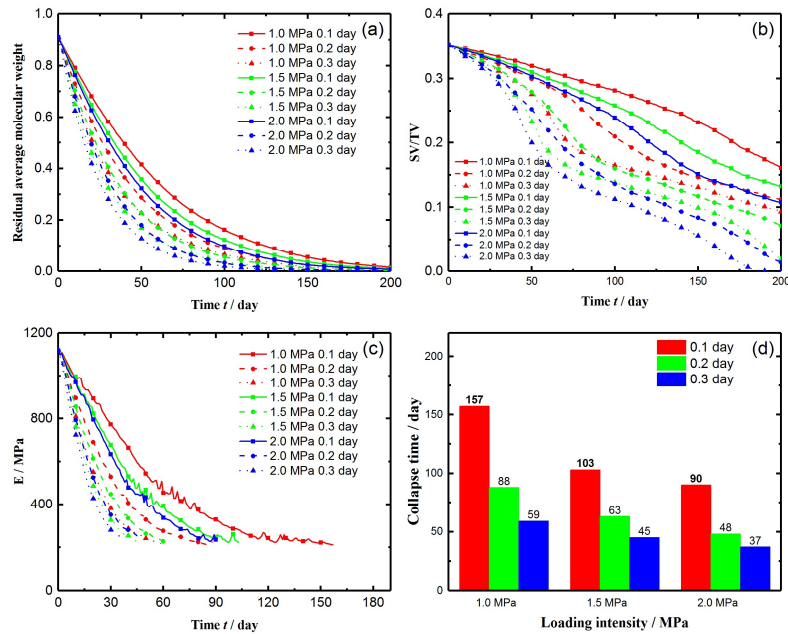


Fig. S2. Degradation of the nine cases of the lattice structure: (a)  $\bar{\beta}(t)$ ; (b) SV/TV; (c) Young's modulus of scaffold-solution system; (d) collapsing time of the system.

$\beta_{\text{threshold}}$  down-regulated by 20%

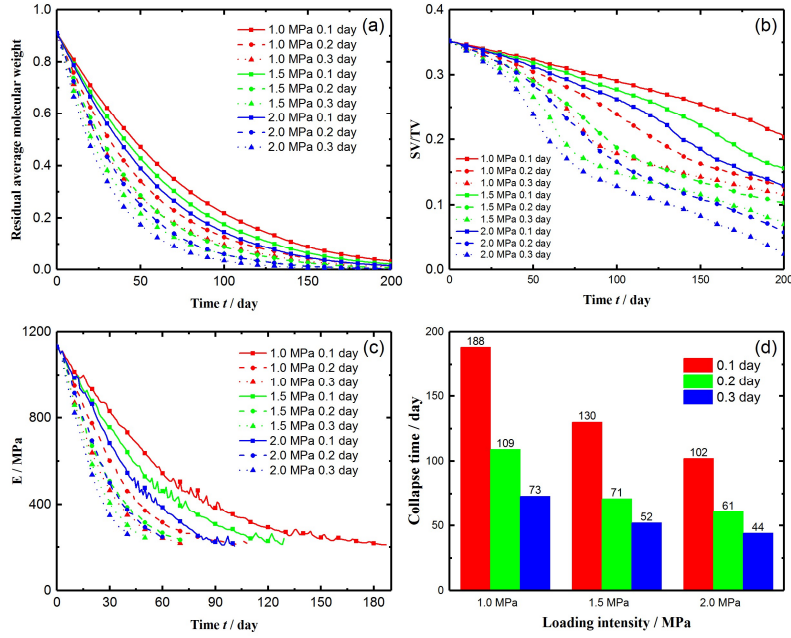


Fig. S3. Degradation of the nine cases of the lattice structure: (a)  $\bar{\beta}(t)$ ; (b) SV/TV; (c) Young's modulus of scaffold-solution system; (d) collapsing time of the system.

$\beta_{\text{threshold}}$  up-regulated by 20%

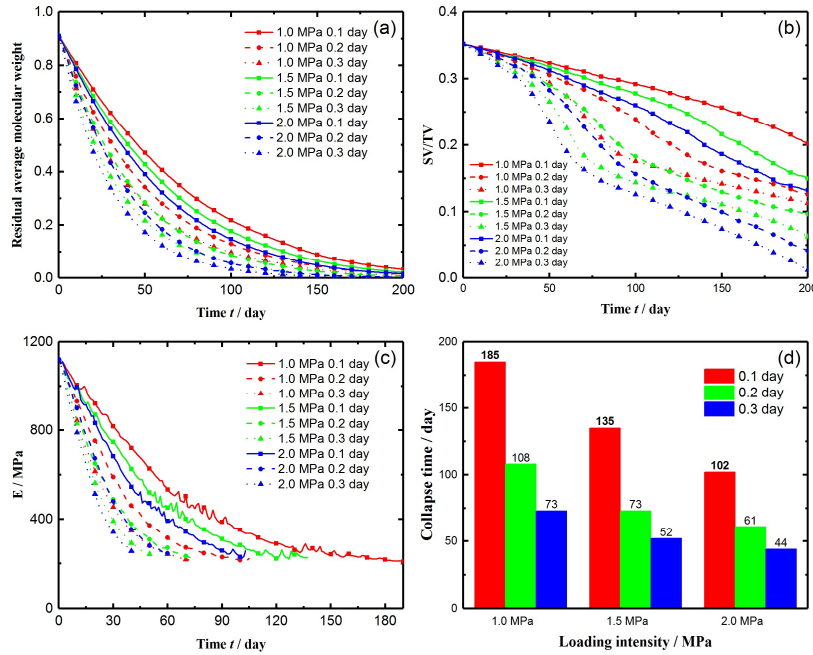


Fig. S4. Degradation of the nine cases of the lattice structure: (a)  $\bar{\beta}(t)$ ; (b) SV/TV; (c) Young's modulus of scaffold-solution system; (d) collapsing time of the system.

$D_0$  down-regulated by 20%

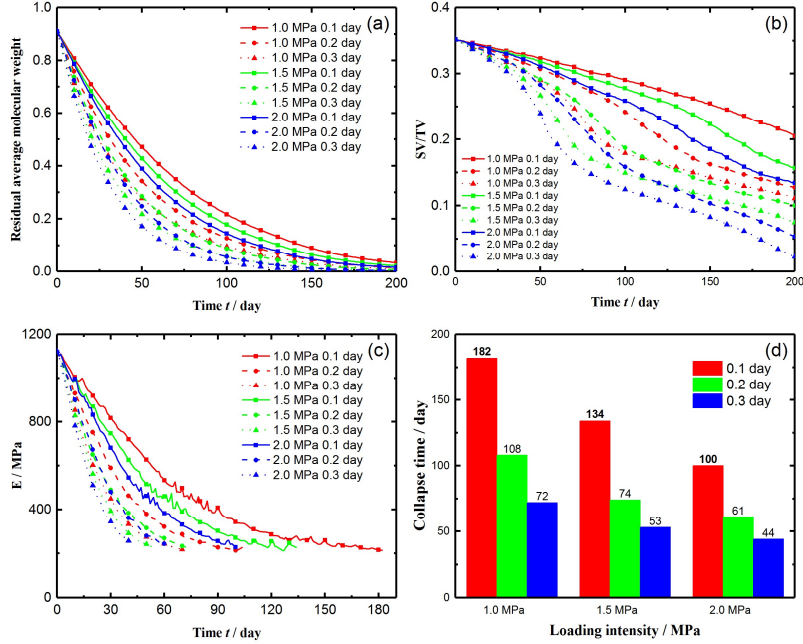


Fig. S5. Degradation of the nine cases of the lattice structure: (a)  $\bar{\beta}(t)$ ; (b) SV/TV; (c) Young's modulus of scaffold-solution system; (d) collapsing time of the system.

### $D_0$ up-regulated by 20%

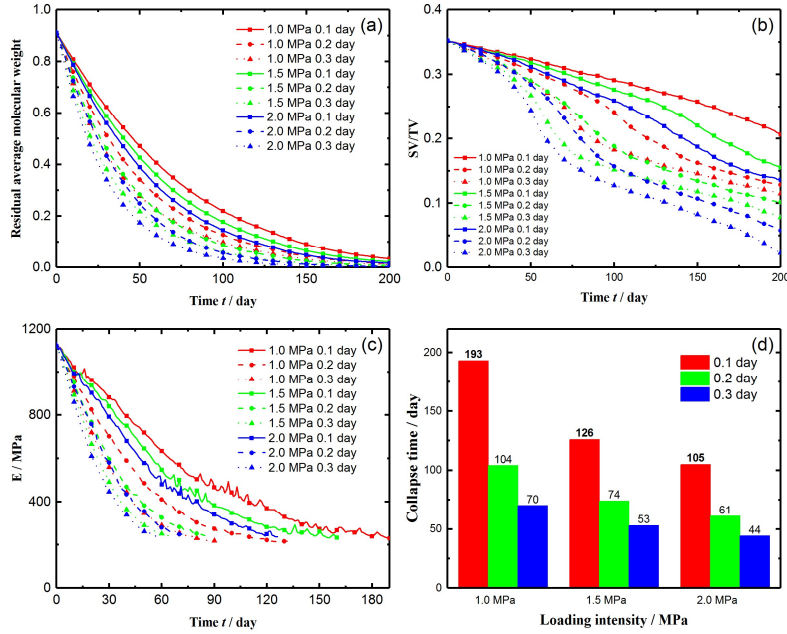


Fig. S6. Degradation of the nine cases of the lattice structure: (a)  $\bar{\beta}(t)$ ; (b) SV/TV; (c) Young's modulus of scaffold-solution system; (d) collapsing time of the system.

### $E_s$ down-regulated by 20%

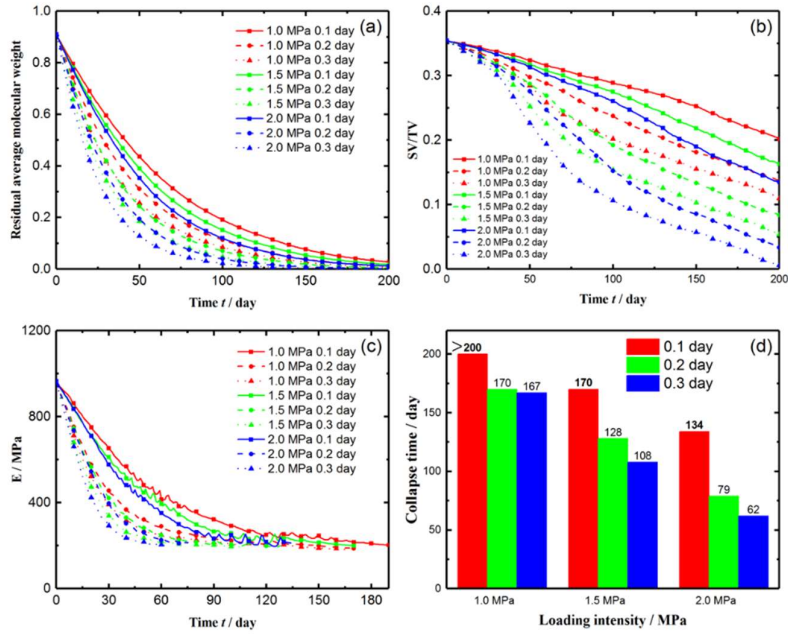


Fig. S7. Degradation of the nine cases of the lattice structure: (a)  $\bar{\beta}(t)$ ; (b) SV/TV; (c) Young's modulus of scaffold-solution system; (d) collapsing time of the system.

**$E_s$  up-regulated by 20%**

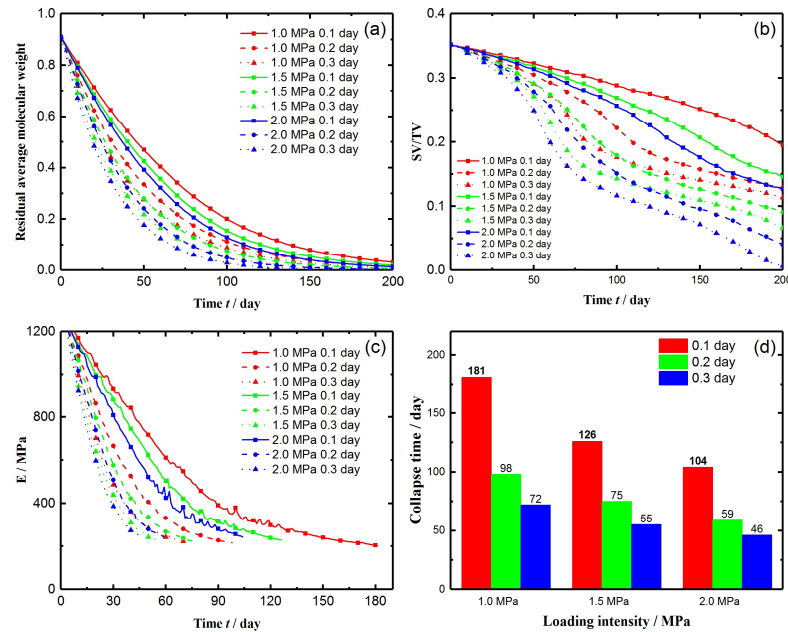


Fig. S8. Degradation of the nine cases of the lattice structure: (a)  $\bar{\beta}(t)$ ; (b) SV/TV; (c) Young's modulus of scaffold-solution system; (d) collapsing time of the system.

**The spherical structures:**

$\lambda_0$  down-regulated by 20%

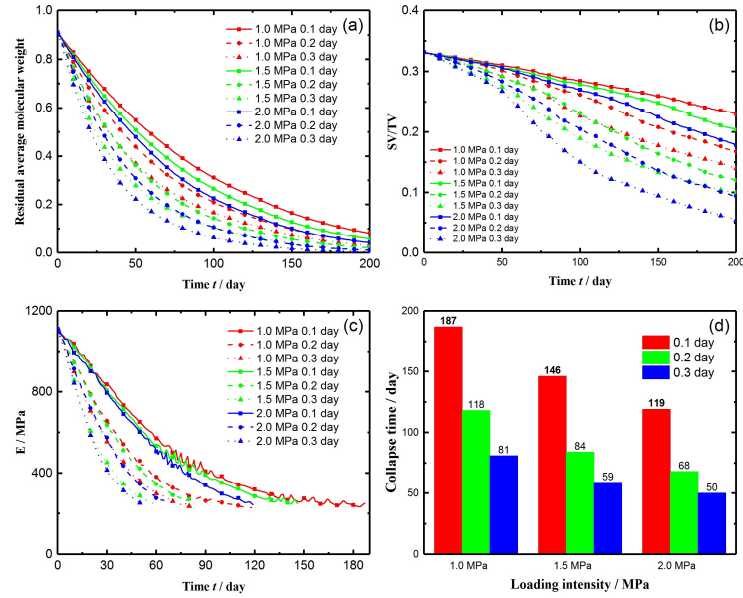


Fig. S9. Degradation of the nine cases of the spherical structure: (a)  $\bar{\beta}(t)$ ; (b) SV/TV; (c) Young's modulus of scaffold-solution system; (d) collapsing time of the system.

$\lambda_0$  up-regulated by 20%

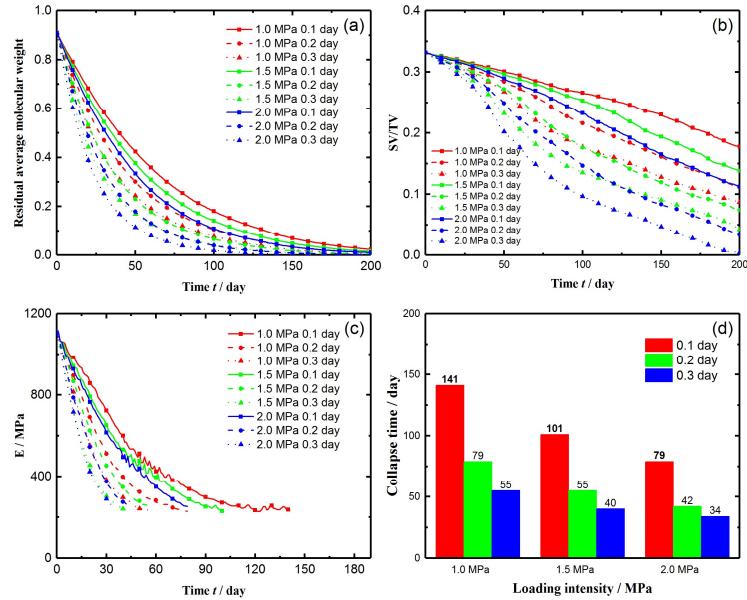


Fig. S10. Degradation of the nine cases of the spherical structure: (a)  $\bar{\beta}(t)$ ; (b) SV/TV; (c) Young's modulus of scaffold-solution system; (d) collapsing time of the system.

$\beta_{\text{threshold}}$  down-regulated by 20%

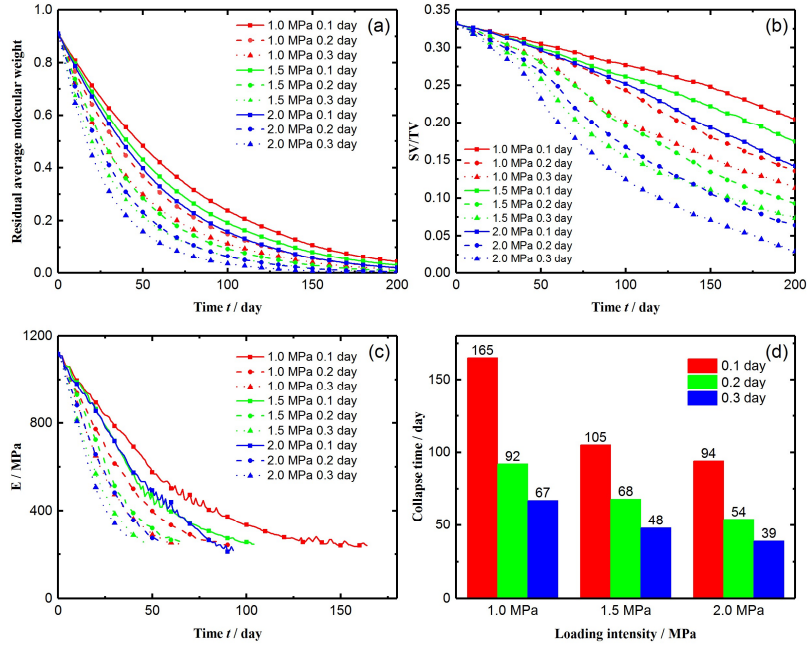


Fig. S11. Degradation of the nine cases of the spherical structure: (a)  $\bar{\beta}(t)$ ; (b) SV/TV; (c) Young's modulus of scaffold-solution system; (d) collapsing time of the system.

**$\beta_{\text{threshold}}$  up-regulated by 20%**

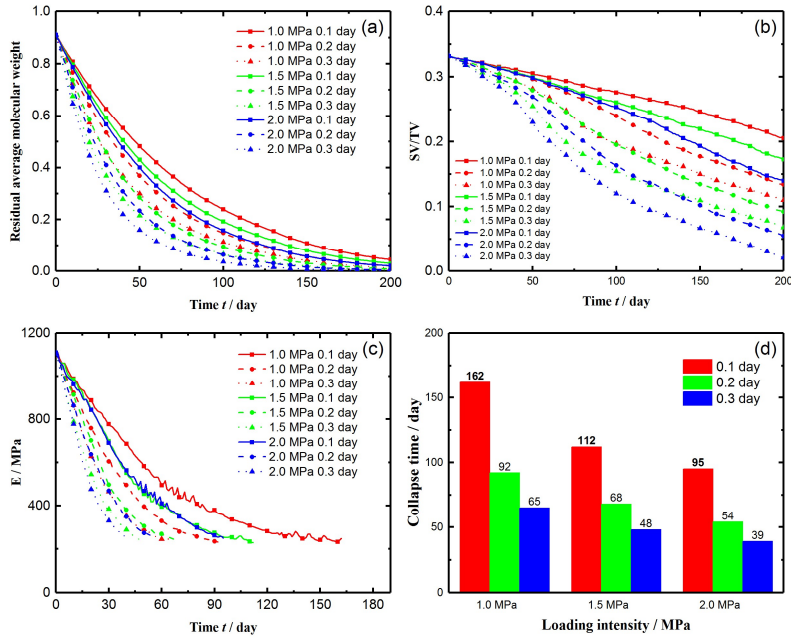


Fig. S12. Degradation of the nine cases of the spherical structure: (a)  $\bar{\beta}(t)$ ; (b) SV/TV; (c) Young's modulus of scaffold-solution system; (d) collapsing time of the system.

**$D_0$  down-regulated by 20%**

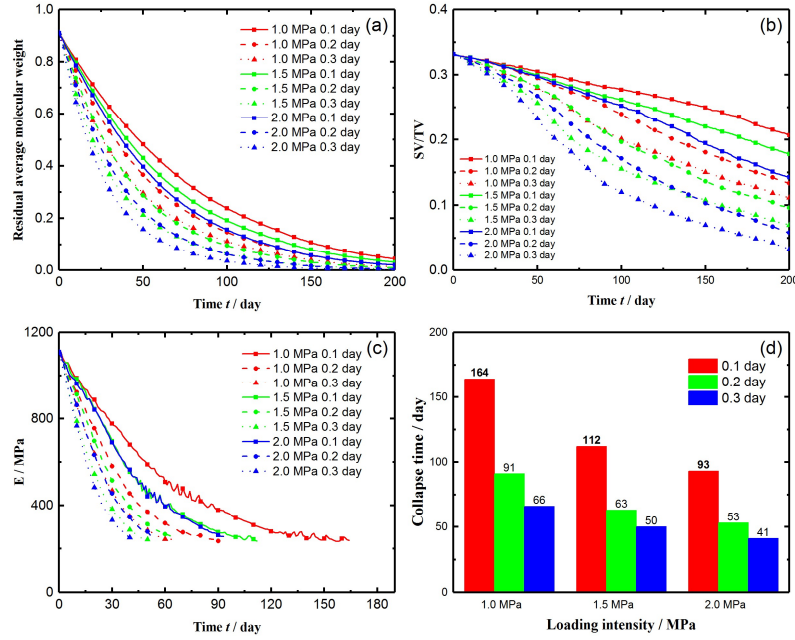


Fig. S13. Degradation of the nine cases of the spherical structure: (a)  $\bar{\beta}(t)$ ; (b) SV/TV; (c) Young's modulus of scaffold-solution system; (d) collapsing time of the system.

**$D_0$  up-regulated by 20%**

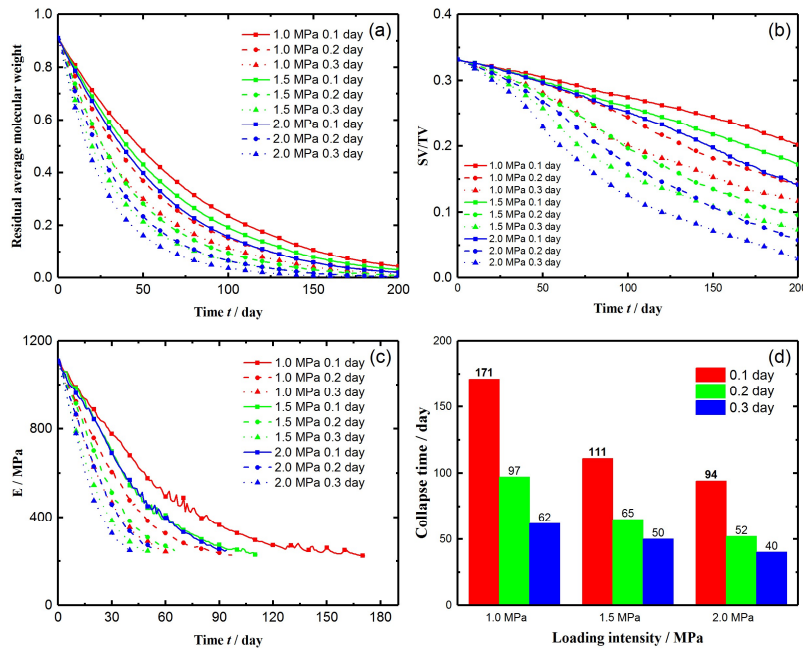


Fig. S14. Degradation of the nine cases of the spherical structure: (a)  $\bar{\beta}(t)$ ; (b) SV/TV; (c) Young's modulus of scaffold-solution system; (d) collapsing time of the system.

**$E_s$  down-regulated by 20%**

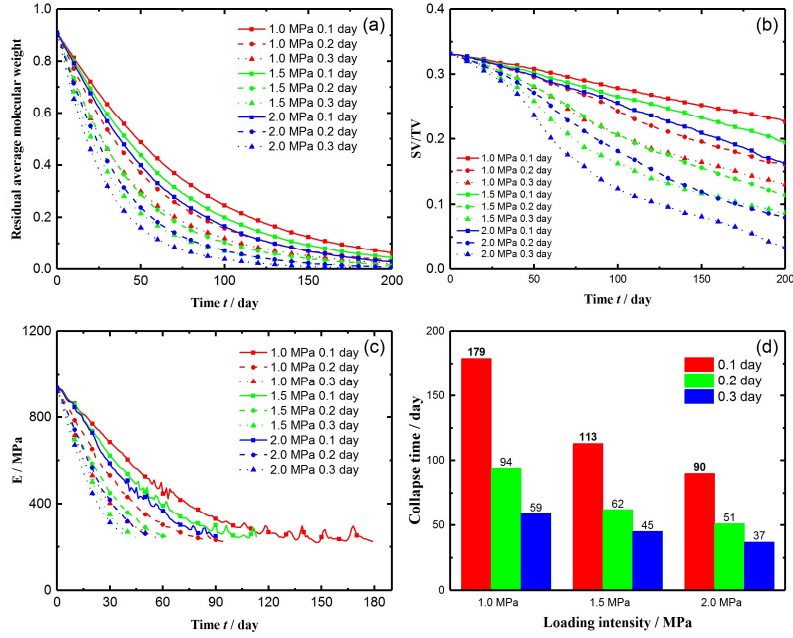


Fig. S15. Degradation of the nine cases of the spherical structure: (a)  $\bar{\beta}(t)$ ; (b) SV/TV; (c) Young's modulus of scaffold-solution system; (d) collapsing time of the system.

### $E_s$ up-regulated by 20%

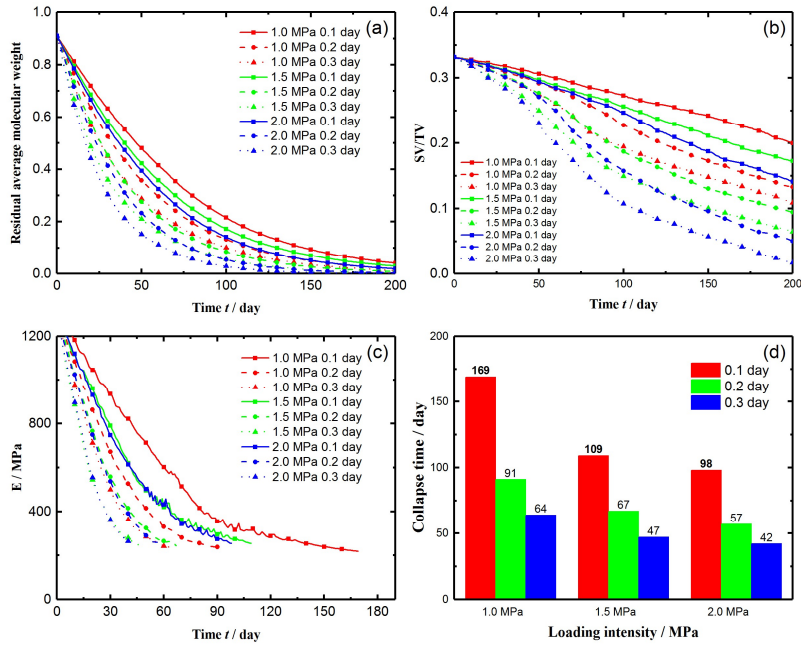


Fig. S16. Degradation of the nine cases of the spherical structure: (a)  $\bar{\beta}(t)$ ; (b) SV/TV; (c) Young's modulus of scaffold-solution system; (d) collapsing time of the system.

### The truss structures

$\lambda_0$  down-regulated by 20%

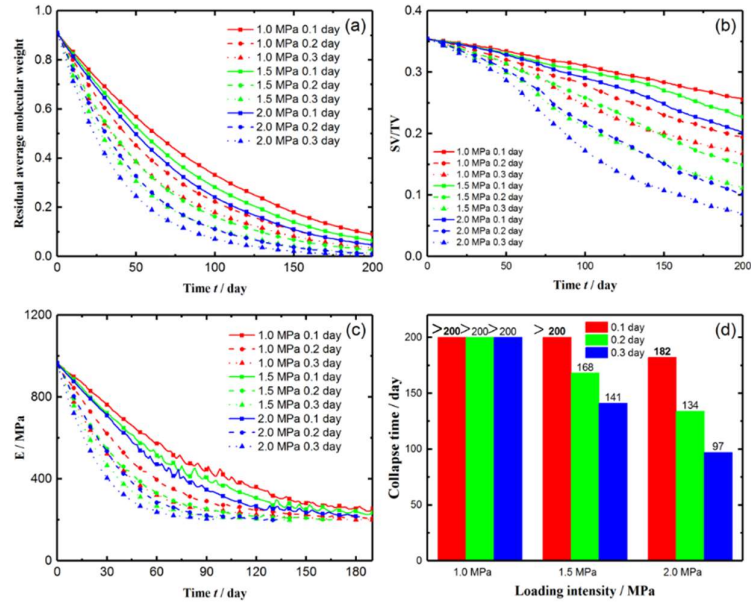


Fig. S17. Degradation of the nine cases of the truss structure: (a)  $\bar{\beta}(t)$ ; (b) SV/TV; (c) Young's modulus of scaffold-solution system; (d) collapsing time of the system.

$\lambda_0$  up-regulated by 20%

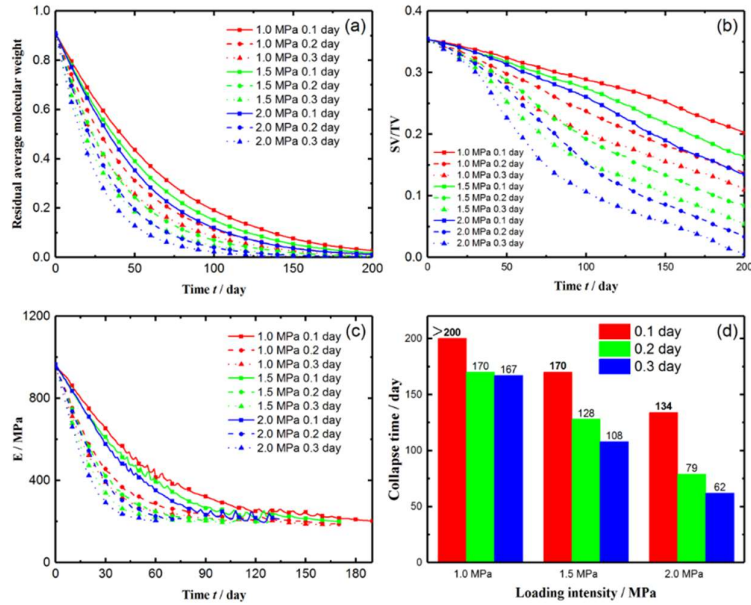


Fig. S18. Degradation of the nine cases of the truss structure: (a)  $\bar{\beta}(t)$ ; (b) SV/TV; (c) Young's modulus of scaffold-solution system; (d) collapsing time of the system.

$\beta_{\text{threshold}}$  down-regulated by 20%

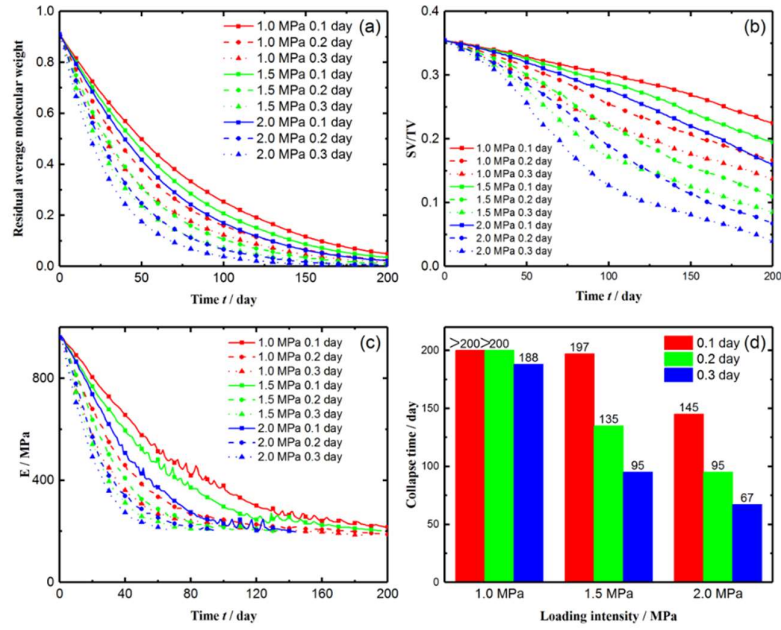


Fig. S19. Degradation of the nine cases of the truss structure: (a)  $\bar{\beta}(t)$ ; (b) SV/TV; (c) Young's modulus of scaffold-solution system; (d) collapsing time of the system.

**$\beta_{\text{threshold}}$  up-regulated by 20%**

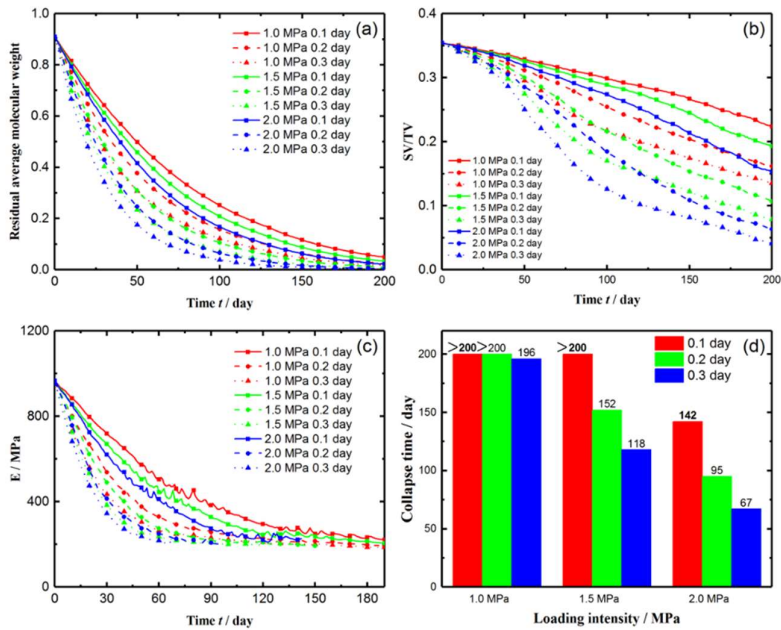


Fig. S20. Degradation of the nine cases of the truss structure: (a)  $\bar{\beta}(t)$ ; (b) SV/TV; (c) Young's modulus of scaffold-solution system; (d) collapsing time of the system.

**$D_0$  down-regulated by 20%**

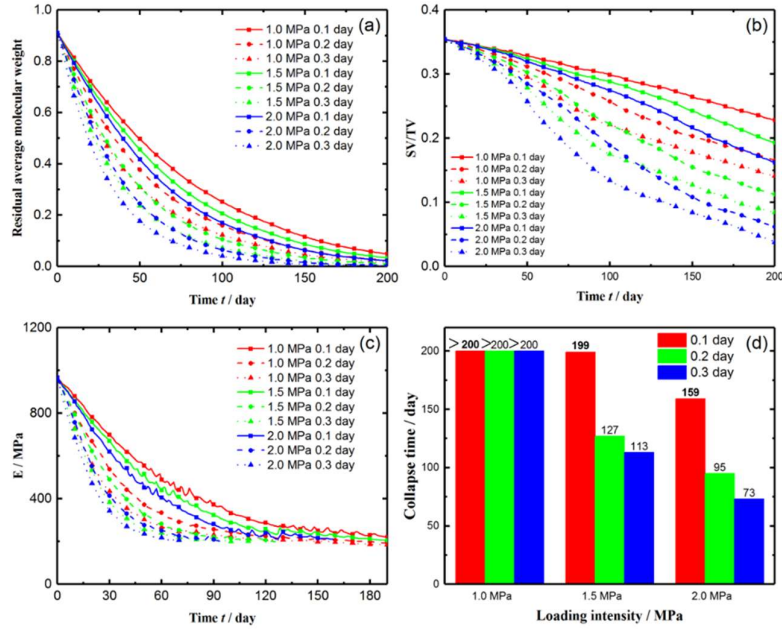


Fig. S21. Degradation of the nine cases of the truss structure: (a)  $\bar{\beta}(t)$ ; (b) SV/TV; (c) Young's modulus of scaffold-solution system; (d) collapsing time of the system.

### $D_0$ up-regulated by 20%

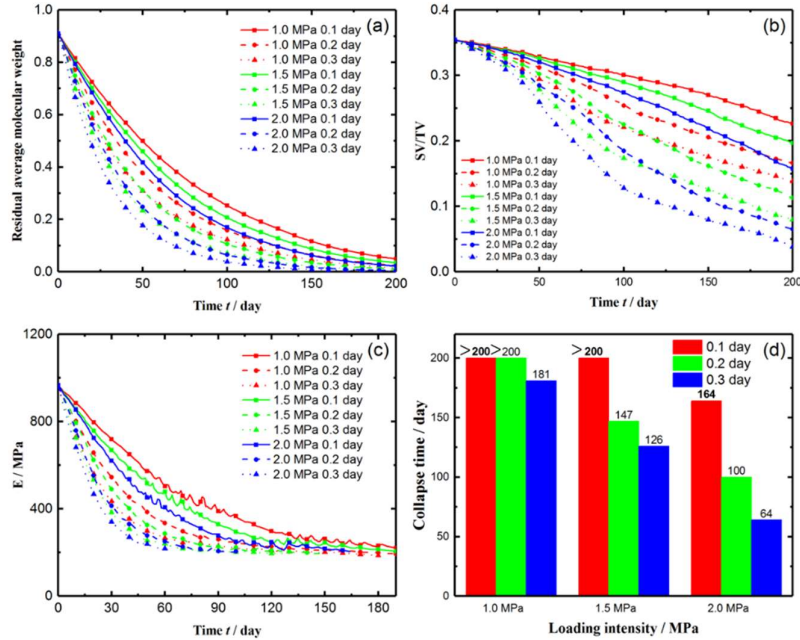


Fig. S22. Degradation of the nine cases of the truss structure: (a)  $\bar{\beta}(t)$ ; (b) SV/TV; (c) Young's modulus of scaffold-solution system; (d) collapsing time of the system.

### $E_s$ down-regulated by 20%

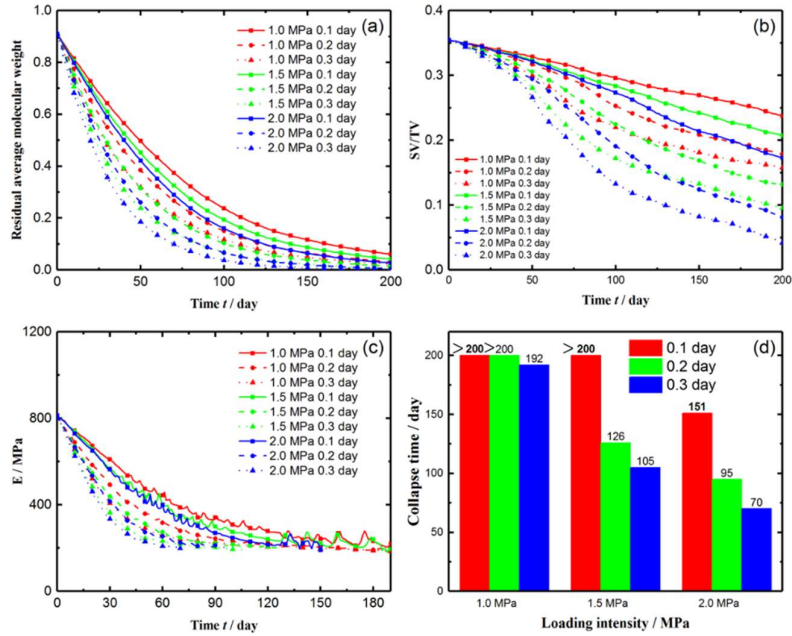


Fig. S23. Degradation of the nine cases of the truss structure: (a)  $\bar{\beta}(t)$ ; (b) SV/TV; (c) Young's modulus of scaffold-solution system; (d) collapsing time of the system.

**$E_s$  up-regulated by 20%**

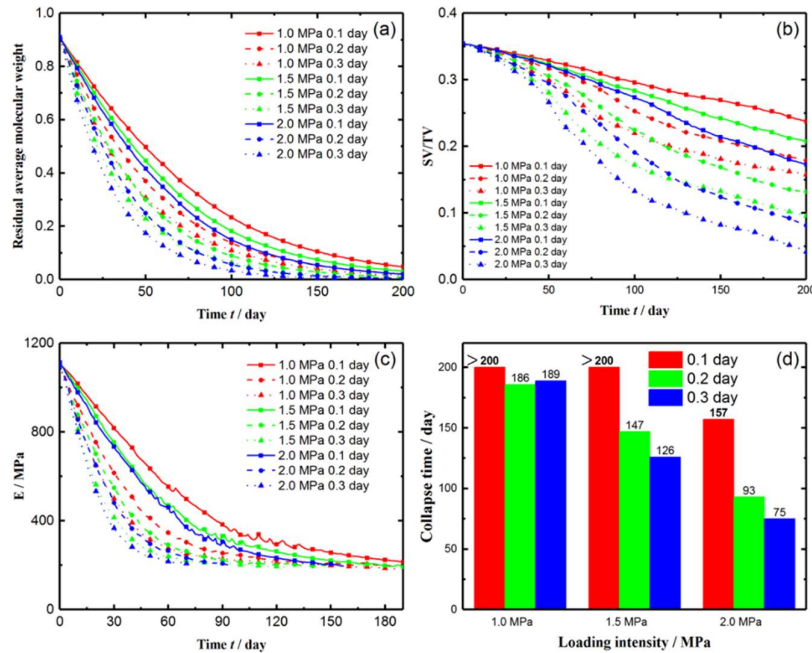


Fig. S24. Degradation of the nine cases of the truss structure: (a)  $\bar{\beta}(t)$ ; (b) SV/TV; (c) Young's modulus of scaffold-solution system; (d) collapsing time of the system.